NOLTR 72-34

A REVIEW OF SPHERE DRAG COEFFICIENTS APPLICABLE TO ATMOSPHERIC DENSITY SENSING

By
Maigonis V. Krumins

18 JANUARY 1972

NOL

NAVAL ORDNANCE LABORATORY, WHITE OAK, SILVER SPRING, MARYLAND

NOLTR 72-34

APPROVED FOR PUBLIC RELEASE;
DISTRIBUTION UNLIMITED

A REVIEW OF SPHERE DRAG COEFFICIENTS APPLICABLE TO ATMOSPHERIC DENSITY SENSING

Prepared by:
Maigonis V. Krumins

ABSTRACT: A comprehensive search has been performed on the drag coefficient of spheres in the Reynolds number range from 5×10^1 to 5×10^4 and for Mach numbers up to 5. This Reynolds-Mach number range corresponds to the range of interest in the falling sphere technique of atmospheric sensing. In this technique, the knowledge of the sphere's trajectory and its aerodynamic characteristics is utilized to obtain the density of the atmosphere. The presently available data have been collected and analyzed as to their validity and applicability to atmospheric density measurements. A new drag table is recommended for use in these measurements. Since the vehicles used for atmospheric sensing are inflated spherical balloons, the question still remains if a factor needs to be applied to correct the drag data measured on idealized spheres for effects, such as those due to surface roughness, surface temperature, out of roundness, etc.

NAVAL ORDNANCE LABORATORY
SILVER SPRING, MARYLAND

NOLTR 72-34 18 January 1972

A REVIEW OF SPHERE DRAG COEFFICIENTS APPLICABLE TO ATMOSPHERIC DENSITY SENSING

This work was funded by the National Aeronautics and Space Administration, Langley Research Center, under Purchase Order No. L-43,531. The project was monitored by Mr. John S. Preisser of NASA, Langley Research Center, to whom the author is indebted for his many suggestions in preparing the report and the thorough critique of its final draft.

The author also wishes to acknowledge the support and the assistance given by Dr. W. Carson Lyons during the initial stages of the study.

ROBERT WILLIAMSON II
Captain, USN
Commander

A. E. Seigel

A. E. SEIGEL
By direction

CONTENTS

ILLUSTRATIONS

TABLE

SYMBOLS

a	acceleration
A	area
C_D	drag coefficient
d	diameter
F	force
I	moment of inertia
k	roughness factor
m	mass
M	Mach number
r	radius
R_d	Reynolds number based on diameter
t	thickness
T_o	stagnation temperature
T_w	wall temperature
V	velocity
x	distance in the direction of velocity vector
ϵ	ratio of thickness to radius of sphere
ω	angular velocity
ρ	density

Subscripts

i	refers to initial condition
i	refers to inside diameter
f	refers to final condition
o	refers to outside diameter
v	refers to the direction of velocity vector
2	refers to conditions behind normal shock

INTRODUCTION

A body falling through the atmosphere may be used to measure the density of the atmosphere, if the aerodynamic characteristics of the body are well determined beforehand and the velocity history of the fall is measured and recorded. A spherical shape has been utilized to probe the upper atmosphere of the earth, since it has the inherent advantage of possessing rotational symmetry, thus eliminating the problems of angle of attack.

Newton's second law, written for a falling body in a simplified form (coriolis acceleration, buoyancy, etc., neglected), is

$$\Sigma F_v = ma_v$$

where v denotes the velocity direction. Since drag is the only force in the velocity direction, the above relation becomes

$$-\text{Drag} = ma_v$$

Applying the definition of drag coefficient

$$C_D = \frac{\text{Drag}}{\frac{1}{2} \rho V^2 A}$$

one gets

$$-\frac{1}{2} \rho V^2 A C_D = ma_v$$

which can be solved for density

$$\rho = \frac{-ma_v}{\frac{1}{2} V^2 A C_D}$$

It is seen that the density of the surrounding atmosphere can be obtained if values for the terms on the right-hand side can be measured. The mass, m, and the area, A, on which the drag coefficient is defined are constant and known before the flight. There have been two methods used to determine the instantaneous velocity,

V, and the acceleration (or rather deceleration in this case), a_V, in the direction of the velocity. The acceleration has been measured directly using built-in accelerometers and then the velocity obtained through integration. The units carrying these accelerometers have been rather heavy and have successfully been used at lower altitudes. To obtain measurements at high altitudes, much lighter, larger diameter bodies need to be used so that the fall rate, as well as the mass, will be low enough to detect density gradients in the tenuous environment. One such object commonly used has been the balloon with a metallic reflector inside so that it can be tracked by radar. With precision, ground-based radar, the position of the falling balloon is determined at each instant of flight. This space-time plot is then differentiated to obtain the velocity history and, again, to obtain the acceleration.

One more quantity needs to be determined before density can be calculated. The drag coefficient of the falling shape must be known at each instant during the fall. It is the subject of this report to investigate the validity of the available data on spherical shapes for use in the falling sphere technique of measuring the atmospheric density. Spheres have been widely used for such measurements, and a considerable amount of experimentation has been performed on this configuration to determine its drag characteristics in different flight regimes. These data have been collected and are analyzed in this report.

In continuum flow, the drag coefficient of a sphere has been described as a function of the Reynolds number and the Mach number. In rarefied gas flow regimes, the Knudsen number is also a significant parameter. The Knudsen number, however, can be expressed approximately as a Mach number - Reynolds number function. The ranges of these parameters that are of interest in the falling sphere technique of measuring the upper atmosphere are as follows:

Subsonic

Mach Number = less than one
Reynolds Number = 5×10^2 to 5×10^4

Supersonic

Mach Number = 1 to 5
Reynolds Number = 5×10^1 to 5×10^3

These regimes are illustrated in Figure 1 by a shaded area. The data in each regime, the subsonic and the supersonic, will be analyzed separately.

SUBSONIC REGIME

The subsonic data may, again, be subdivided into two main categories, the incompressible and the compressible. The incompressible

data are obtained by performing experiments in an essentially incompressible fluid, like water, or they may be obtained in a gas, under conditions such that the compressibility effects are negligible. The upper limit under which a gaseous flow customarily has been considered incompressible is when the Mach number is equal to or less than 0.3. Above that Mach number, the drag coefficient is also a function of Mach number in addition to being a function of Reynolds number alone.

Incompressible Data

Figure 2 shows the Reynolds number coverage of past experiments available in open literature on subsonic sphere drag and the range of applicability for the falling sphere atmospheric sensing technique. A work that describes the drag coefficient over a wide range of Reynolds numbers is that of Wieselsberger, references (1) and (2). In this investigation, the drag coefficient of a sphere was measured over a range of Reynolds numbers from 8×10^2 to 9×10^5. These experiments were performed in a wind tunnel at Mach numbers less than 0.1 and, together with Allen's measurements in water, reference (3), at Reynolds numbers below 2×10^2, define what will be called the Wieselsberger curve or the incompressible curve.

Transition from laminar to turbulent flow in the boundary layer takes place at Reynolds numbers approximately between 2×10^5 and 5×10^5, which is accompanied by a significant and a rather abrupt decrease in the drag coefficient. This phenomenon has attracted considerable attention. In references (4) through (8), different phenomena affecting transition in the boundary layer are investigated. In these references, the effects of tunnel turbulence, Mach number, surface roughness, etc., are studied. Tripping of the boundary layer and its effects are also described, and the resulting changes in the pressure distribution around the body are measured in the critical Reynolds number range. Since the critical Reynolds number is outside the range of interest in the falling sphere technique of atmospheric sensing, a detailed analysis of these experiments will not be made.

The range of Reynolds numbers of interest at subsonic Mach numbers is between 5×10^2 and 5×10^4. Seven investigations have been performed in this region, satisfying the incompressibility condition, and they are described in references (1), (2), (3), (9), (10), (11), and (12). All of the measured data points from these references are reproduced on a C_D versus R_d plot in Figure 3. The solid line is reproduced from Wieselsberger's paper, reference (1), as well as the data points substantiating this line from references (2) and (3). Wieselsberger's experiments were performed in a wind tunnel with the model supported on wires. The force on the sphere was determined by the amount the model is displaced on the support system against counterweights.

The other incompressible data in air were obtained by dropping spheres from towers (Shakespeare, reference (12)) and in mine shafts

(Lunnon, reference (10)). These data differ considerably, especially the ones obtained in mine shafts from the wind-tunnel experiments. This can be attributed to the difficulties that are encountered when timing the fall of a body over a certain height. As is pointed out by the author in reference (12), the accuracy of the experiments heavily depended on the atmospheric conditions. The most consistent results from the tower drop tests were obtained on dull, cloudy, and still days. Clear weather invariably brought more scatter into the data. This was attributed to drafts. The models used were hollow celluloid spheres, which were weighted with lead to obtain the desired mass. Sphericity of these spheres, which were such that they could be opened to insert the lead, can also be questioned. The data obtained in mine shafts (Lunnon, reference (10)) are below the wind-tunnel measurements by as much as 20 percent. Here again, air currents in the shaft, as well as temperature variation with depth, could be contributing to the inaccuracy of the measurements.

There are three references describing results of measurements performed in water. In 1900, Allen, reference (3), measured drag by dropping small steel spheres in water. The measurements are shown with a symbol, ◇, in Figure 3 and are seen to be from 10 percent to 17 percent below the wind-tunnel curve established by Wieselsberger. These, incidentally, fall in line with Shakespeare's measurements obtained by dropping spheres in mine shafts. Liebster, reference (9) (◇), performed similar experiments to those of Allen. These data have relatively high scatter among themselves and differ from Wieselsberger's curve by as much as 17 percent at $R_d = 1.15 \times 10^3$. Better agreement with the wind-tunnel data was obtained by Lunnon, reference (10) (□), also by dropping spheres in water. There is some discrepancy at the higher Reynolds numbers ($R_d > 10^4$), indicating that the rise in C_D with Reynolds number is at a higher R_d than in the wind-tunnel tests. It seems that it is more difficult to obtain a good drag coefficient in a water drop test than it appears at first. In sphere drop tests at NOL, where the cavity behind the sphere was the center of study and not the drag coefficient, it was observed that a sphere never descends in a straight line. It always falls in a random trajectory similar to the path of a knuckle ball. This kind of trajectory is caused by the vortices being shed at the separation point which varies along the periphery of the sphere, thus altering pressure distribution and the direction of the fall. The vortex frequency has been studied by Moller, reference (13), and the Streuhal number correlated with Reynolds number. Excellent photographs of the vortices are included in the paper. In all the early experiments mentioned above, the length of fall was timed between different heights without regard for the direction of the velocity vector of the center of gravity at each point during the fall. In a wind-tunnel test, the drag force is measured in the direction of the velocity vector; while in the drop test in water, this condition was not satisfied. To obtain an accurate drag coefficient from a drop test, one needs to determine the trajectory of the sphere and base the drag calculations on the actual fall path in a manner similar to modern data reduction programs in a ballistics range.

Compressible Data

Recent measurements of sphere drag were performed in a ballistics range by Goin and Lawrence, reference (11). These tests were made in air and the compressibility effects investigated by covering a Mach number range between 0.2 and 0.98. The results are presented in Figure 4. In this figure, Wieselsberger's incompressible curve is reproduced from Figure 3 and the data at higher Mach numbers presented by different symbols. Data at Mach number 0.2 (●) in a ballistics range show excellent agreement with the curve established by Wieselsberger at $M < 0.1$ in a wind tunnel. The maximum deviation is at $R_d = 3.7 \times 10^3$ and is approximately 1.6 percent. At other Reynolds numbers where data were obtained, they fall directly on the Wieselsberger curve. The next set of data measured by Goin and Lawrence is at $M = 0.33$ (▲). At low Reynolds numbers there is a very small, but a definite effect of Mach number on C_D, but at $R_d \simeq 10^4$, the effect is quite pronounced. A four percent higher C_D was measured at $M = 0.33$ (▲) than at $M = 0.2$ (●). This leads one to conclude that the compressibility effects are noticeable at slightly lower Mach numbers than the previously accepted value of 0.3, which was arrived at by allowing a change in density, $\Delta\rho/\rho$, equal to 0.05, reference (14). The Mach number range in these tests was extended to 0.98. At $M = 0.46$ (◣) and $M = 0.60$ (◉), the data cover a Reynolds number range between 2×10^2 and 10^4. At Mach numbers of 0.75 (◆), 0.89 (◆), and 0.98 (⬢), the Reynolds number coverage is rather limited. The compressible data do seem to follow the same slope as the incompressible curve so that the effect of compressibility (or Mach number) can be quite well established at least in a narrow band of Reynolds numbers. The lowest pressure in the ballistics range during any one of the shots was 7 torr. It should be possible to measure pressure at this level to within .5 percent, and, with a three percent slowdown during the flight, the error in dV/dx should be below two percent. The overall accuracy in the drag coefficient should be within ± 2.5 percent at the most.

There has been one more significant work done in an attempt to determine the drag of spheres at subsonic Mach numbers. This is the work of Heinrich and his co-workers at the University of Minnesota, references (15) and (16). Wind-tunnel tests at Mach numbers between 0.39 and 0.86 have been performed in the Reynolds number range between 10^3 and 2.5×10^3. A 0.5-inch-diameter sphere made of teflon was used throughout the tests. Data also were obtained on related, oblate, and prolate spheroids at selected Mach numbers and Reynolds numbers, as well as on the effect of sphere rotation on its drag coefficient.

The measured drag coefficients for spheres have been included in Figure 4. Four data points measured at Mach number 0.39 (◭) generally agree, within the expected accuracy of measurements, with the data obtained in a ballistics range at Mach numbers $M = 0.33$ (▲) and 0.46 (◣). These data agree also in the trend of decreasing value of drag coefficients with increasing Reynolds number. As the

Mach number increases, this similarity in the two sets of data ceases. At Mach number 0.66 (◇), the wind-tunnel data are below the values at M = 0.6 (●) of the ballistics range data and, furthermore, do not agree with the trend established by the incompressible measurements. The wind-tunnel data seem to be independent of Reynolds number. At higher Mach numbers, specifically, M = 0.74 (○), the data indicate a reverse trend, i.e., increasing drag coefficient with increasing Reynolds number. At still higher Mach numbers, like M = 0.82 (△), the trend in the data seems to have reversed again, showing a slope similar to that of the incompressible curve, although not as steep; while at Mach number 0.86 (▲), the trend cannot be determined, owing to larger scatter in these data.

The accuracy of the wind-tunnel measurements mainly depends on the accuracy with which pressure can be measured. The errors introduced by the force balance used to measure the drag force are small compared to the accuracy of the pressure measurement at very low levels. To obtain the Reynolds number variation covered by the data, the pressure was the only parameter varied, since the same size model was used throughout, and the Mach number was kept constant for a given set of data. The highest possible error is at the low Reynolds number, since the pressure there is very low. It has been estimated by authors of reference (17) that the maximum error at the low Reynolds numbers is five percent and at the high Reynolds numbers, one percent. The scatter in these data is as high as 3 to 4.5 percent. These wind-tunnel and ballistics range data of reference (11) are repeated in Figure 5 to better compare the two sets. The wind-tunnel data are shown in open symbols and the ballistics range data, in solid. Error bars have been added to each data point. A linear variation in the magnitude of the error was assumed for the wind-tunnel data from five percent at $R_d = 10^3$ to one percent at 2.4×10^3. A constant two percent error was applied to the ballistics range data. Although the error bars in the two sets of data overlap at certain Reynolds numbers, it is clear from Figures 4 and 5 that the ballistics range data show a much stronger effect of Reynolds number on C_D than the data of Heinrich obtained in a wind tunnel. This discrepancy has been speculated by Heinrich, et al, to be due to tunnel wall interference, model support interference, or apparent mass effects, which are a result of a change in kinetic energy of the model as it flies and decelerates in a ballistics range. These are certainly valid arguments to explain the differences observed in the measurements, but it is doubtful whether they have strong enough influences to cause such large differences as are indicated by the data. In a recent work by Zarin, reference (18), the effect of free-stream turbulence has been studied on the drag coefficient of spheres in the Reynolds number region identical to the one covered by the data of Heinrich, et al, reference (16), and Goin and Lawrence, reference (11). In Figure 6, one of the figures from reference (18) is reproduced. It shows this effect on various size models (the turbulence providing screen was kept the same for all of the models, 16 x 16 x .001 inch, therefore, the ratio of turbulent eddy size to model size was altered by using

models of different diameters). The effect of free-stream turbulence on sphere drag seems to be quite pronounced, showing the reverse trend in C_D with Reynolds number to the incompressible curve that was observed in the Heinrich, et al, reference (16), wind-tunnel data. Although no turbulence level measurements are available for the tests in reference (16), it is possible that the disagreement between that data and the equivalent data obtained in the ballistics range, reference (11), is largely due to turbulence in the free stream. In a ballistics range, the atmosphere should be considered quiet since the currents and pulsations from the action of the vacuum pumps used to evacuate the range tube to the desired pressure level are small. Furthermore, the countdown procedures usually require several minutes between the time the pumps are shut off and the time of fire during which any of the disturbances should damp out.

Summary of Subsonic Data

In summary, the subsonic drag data on spheres have been analyzed and the experimental results compared with one another. The incompressible curve seems to be rather well defined by three independent methods. At low Reynolds numbers, Allen's measurements in water, reference (3), on air bubbles, and spheres made of amber agree well with Goin and Lawrence's, reference (11), ballistics range results. Liebster's, reference (9), drop tests in water are hampered by excessive scatter and really do not help much in defining the curve. At Reynolds numbers higher than 800, Wieselsberger's wind-tunnel data, reference (1), agree well with Goin and Lawrence's measurements as well as Lunnon's, reference (10), water drop test results. The latter begin to deviate from the wind-tunnel curve above $R_d = 2 \times 10^4$. Except at these higher Reynolds numbers, where data from drop tests in water and air and the wind-tunnel experiments differ quite markedly and ballistics range data are not available, the curve established by Wieselsberger from his own and Allen's measurements in reference (1) can be considered to be adequate and accurate to within 1.5 percent for defining the incompressible curve for spheres. For Reynolds numbers above 2×10^4, additional testing, particularly in a ballistics range, is necessary to define the drag coefficient.

The compressibility effects have been investigated by two researchers, each giving quite different results. Goin and Lawrence's, reference (11), measurements follow the general trend in variation with Reynolds number established by the incompressible data, while the Heinrich, et al, reference (16), measurements do not. For this reason and also that the ballistics range data have, in this case, smaller error bars than the ones from a wind tunnel, the Goin and Lawrence data should be considered to define the drag coefficient at Mach numbers above 0.2. This Mach number should be considered as the upper limit of incompressibility.

SUPERSONIC REGIME

Experimental Data

As it was in the case of subsonic flow, the Reynolds number regime that has attracted the most attention in previous investigations is outside the Reynolds number region of interest in the falling sphere technique of atmospheric sensing. The only areas where theoretical calculations have been made of sphere drag are in the very large Knudsen number region, where the gas is highly rarefied and the free molecular flow assumptions are satisfied. Experimental measurements in this area are very difficult to perform because of the very small forces on the body and the necessity for measuring extremely low values of pressure. Most of the experimental investigations have been performed in the Reynolds number region of 10^5 - 10^6. Here, on the other hand, no reliable theoretical methods have been developed for calculating the drag, indicating the complexity of the continuum theory. The range of interest in the falling sphere experiments is $50 < R_d < 5 \times 10^3$ and Mach numbers up to 5. This regime is characterized by thick boundary layers and, therefore, large viscous contributions to the total drag. The region is shown on a Reynolds - Mach number plot in Figure 1 from which one sees that all of this area is in the slightly rarefied gas flow regime of slip and transitional flows. Slip flow regime is defined as that for which the velocity at the wall is no longer zero, as in the case of continuum flow, but retains the other properties of continuum flow. Transitional regime is an area between slip flow and free molecular flow regimes where properties generally are not well defined and remain unknown.

Figure 7 shows the Reynolds number coverage of past experiments available in open literature on sphere drag between Mach numbers 1 and 5 and also shows the range of applicability in the falling sphere atmosphere sensing technique. As was pointed out above, numerous investigations were made in the Reynolds number region of 10^5 - 10^6. This is where, at low subsonic Mach numbers, the transition in the boundary layer of the sphere took place, which was accompanied by an abrupt reduction in total drag. This phenomenon was found to diminish at higher subsonic Mach numbers and completely disappear at supersonic Mach numbers. This is illustrated in Figure 8, which has been reproduced from reference (8). This region, however, is outside the Reynolds number range of interest in the falling sphere technique and will not be discussed further. Relatively few investigations have been made in the Reynolds number region between 50 and 5×10^3. These will be studied and discussed in detail.

The most comprehensive investigation covering the Reynolds number region of interest was performed by Aroesty, reference (19). The objective of these wind-tunnel measurements was to gather drag data on spheres in the supersonic rarefied gas regime and to study

the effect of heat transfer at the surface of the sphere on drag, as the sphere wall temperature was reduced from 300 degrees K to 80 degrees K during a test in the wind tunnel. A large number of drag measurements were made. The data near Mach number 2 have been replotted in Figure 9. In reference (19), all data between Mach numbers 1.619 and 2.183 were plotted together. To see if there is a Mach number effect over this region, these same data were subdivided into smaller Mach number groups in Figure 9. Distinction was also made as to the number of wires holding the sphere. The main purpose for such a plot is to see if there are trends with Mach number and if there are consistent support effects.

Because of the relatively large scatter in the data, they were statistically fitted to an equation of the form

$$C_D = A + B/\sqrt{R_d} + C/R_d$$

This equation is represented by the solid line in Figure 9, which is reproduced from a figure in reference (19).

It appears that the fitted curve has somewhat more curvature than the data band and does not represent the data in the Reynolds number region between 50 and 300. This really is subject to the equation chosen and the weighting of the data in the statistical method applied to determine the constants (A, B, and C) in the equation. The maximum width of the scatter band on percentage basis is ±7 percent from a faired curve through the data. Since the fitted line does not follow the scatter band directly in the middle, the error bars at Reynolds number 150, for instance, give a value for $C_D = 1.31 \, {}^{+12.5\%}_{-\ 1.5\%}$ and at Reynolds number 700, $C_D = 1.1 \, {}^{+4.5\%}_{-7.8\%}$. There are several reasons given in reference (19) for the relatively large scatter. First of all, there is an uncertainty as to the magnitude and effect of the non-uniformities in the flow produced by the nozzle. This may be particularly important at $M \simeq 2$, where these disturbances may affect the structure of the flow surrounding the sphere and may cause significant variations in the base drag. It is pointed out by the author in reference (19) that the nozzle used for $M \simeq 2$ test was the least uniform of all the other nozzles used for the higher Mach number tests. It has also been found that in low Mach number tests, when thick boundary layers are present, the results are sensitive to other obstructions in the flow such as shields and pressure probes. It was also found that means of holding the model in the test section had an effect on the drag measured. In all these tests, the spheres were wire supported. As can be concluded from Figure 9, the three-wire mounted model consistently possessed a slightly higher drag coefficient than the four-wire mounted model. This was only observed for the smaller size models used, while the one-inch-diameter model did not show this phenomenon. Another effect observed was, as pointed out in reference (19), that

there was a non-systematic variation in drag with the size of the model at a fixed value of Reynolds number. These effects look very much like those studied by Zarin, reference (18), in the subsonic regime, where the drag was found to be a function of free-stream turbulence and the relative size of the turbulent eddies to model diameter. Of course, there was the ever-present non-uniformity in the nozzle, as well as the model and its support assembly effects. All these contribute to the widening of the scatter band. Except for a definite effect of the number of support wires used on models of certain sizes, although overlapping does occur, no systematic variation was detected with either Mach number or model diameter. Therefore, the width of the scatter band of +7 percent should be considered as the maximum uncertainty in the data.

Results from other investigations are presented in Figure 10. Aroesty's data, reference (19), are represented by the solid line which is the same as the one in the previous figure and the scatter in these data represented by the two dashed lines. Ten years before Aroesty's work, experiments were performed by Kane, references (20) and (21), in the identical Berkeley Low Density Wind Tunnel as was used by Aroesty. The reason for repeating these experiments later by Aroesty, as stated in reference (19), is that there was some uncertainty in interpreting the various pressure probe readings in the low Reynolds number regime. Although the force measurements in the earlier experiments are reported to be quite good, the values of C_D and Reynolds number may, therefore, be questionable. Kane's data are plotted point-by-point in Figure 10. They are again subdivided into smaller Mach number groups to check for Mach number effects. None were found. The sphere sizes varied between 0.10 inch to 1.00 inch in diameter and were supported on circular section rods normal to the flow direction. No model size effects were observed in these experiments as well. Kane's results agree quite well with those of Aroesty at lower Reynolds numbers, where they were considered of questionable accuracy, but show a systematically higher value of drag coefficient in the higher Reynolds number range where good agreement between the two sets of measurements was expected.

Another investigation performed in the same Berkeley Low Density Wind Tunnel is that by Sherman, reference (22). The principal reason for doing these tests was to investigate whether the cross-stream support rod affects the sphere boundary layer and, therefore, the drag. In these tests, the sphere was supported on a similar rod as before (references (20) and (21)) but held the sphere from the back, so that the rod was immersed in the separated flow region and in the wake behind the sphere. Data obtained with this support show a somewhat lower value of drag coefficient at low Reynolds numbers than the wire-held sphere drag data of Aroesty and the cross-stream rod support of Kane. At higher Reynolds numbers, Sherman's data are above those of Aroesty and agree quite well with those of Kane.

It can be concluded that all three investigations in the identical facility at Berkeley really show the same difficulties in the measurements. They show that at $M \simeq 2$ there is no definite discernable trend with small changes in Mach number ($1.62 < M < 2.8$), that there is an effect of model size, but an inconsistent one, and that the method of supporting the sphere does affect the measurements considerably, but that there is no way to eliminate it from the measured data.

There is one more reference where drag measurements on spheres were made in a wind tunnel and results reported. This is the work of Heinrich and his co-workers at the University of Minnesota, reference (16). These measurements are shown in Figure 10 with a square symbol (◪, ■, □) and are separated according to Mach number. Mach number 1.5 (◪) and 2.5 (□) data show a definite and consistent effect of Mach number on drag, with $M = 1.5$ having the higher C_D values. The Mach number 2 (■) data, however, intersect both the lower and higher Reynolds number data. Furthermore, the data at low Reynolds numbers are estimated in reference (16) to have maximum error as high as 27.9 percent for $M = 1.5$ and $R_d = 243.6$ and about 10 percent for $M = 2.0$ and 2.5 and $R_d = 400$, thus severely weakening the above conclusion of C_D dependency on Mach number. The data at higher Reynolds numbers seem to agree quite well with those of Kane, references (20) and (21), and Sherman, reference (22).

The sphere drag data described so far were obtained in wind-tunnel facilities. Some tests have been performed in a ballistics range at the Naval Ordnance Laboratory by May, reference (23), and May and Witt, reference (24). In the former work, spheres of sizes varying from 1/4 to 1/32 inch in diameter were flown. Since the smaller size model could not be detected as it flew in the range to trigger the shadowgraph stations, the spheres were launched in clusters that included some 1/4-inch-diameter spheres to assure triggering. In order that the spheres would slow down approximately at the same rate, the ballistic coefficient, W/C_DA, was matched as closely as possible by using different density materials for the different size models. Up to 12 spheres were launched simultaneously. Interference between the models was expected, but there was enough dispersion between the spheres that some of them were separated far enough from the rest so they could be considered undisturbed. Only the ones that are reported to appear beyond suspicion were replotted in Figure 10. This was judged from the relative position of the spheres on two orthogonal shadowgraph plates at each station along the length of the flight. Since there is a rather large variation in Mach number in these data, they were subdivided into two groups in Figure 10, between Mach numbers 1.81 and 2.67 (●) and between 3.18 and 3.45 (◭). As can be seen, the scatter in the data is too high to help to confirm any of the wind-tunnel measurements in this Reynolds number region, where considerable discrepancy between the different test results exists. Neither can one conclude from these ballistics range data that there is a Mach number effect between the lowest (1.81) and the highest (3.45) Mach numbers.

In another test in the same facility by May and Witt, reference (24), each sphere was launched one at a time. These data are at higher Reynolds numbers than the previous set, actually outside the range of interest to the falling sphere technique for measuring the density of atmosphere, but because of the reduced scatter in these data, they do help to define the drag coefficient at the higher Reynolds number end. As can be seen in Figure 10, these measurements are somewhat lower and support the data of Aroesty, reference (19), rather than those of Kane, references (20) and (21), and Sherman, reference (22), which showed higher drag coefficient values.

Experimental data at higher supersonic Mach numbers are presented in Figure 11. At around Mach number 4, they come from two sources, Aroesty, reference (19), and Wegener and Ashkenas, reference (25). Actual data points from the former reference are not shown, but are represented by a regression curve reproduced from a figure in reference (19) and shown by a solid line, while the spread in measurements is indicated by the dashed lines. The data from the latter reference are shown by an open circle (O) which were also obtained in a wind tunnel. The agreement between the two sets is very good. The Wegener and Ashkenas data are somewhat below the fitted curve of Aroesty's data between Reynolds numbers 1.5×10^2 and 5×10^2, but do fall almost entirely within the lower half of their scatter band. Also included in Figure 11 are the results of measurements of around Mach number 6 by Aroesty. The data are represented by the fitted regression curve and the scatter in the data by dotted lines. The quality of the data seems to be improved at the higher Mach numbers, the maximum width of the scatter band at $M = 6$ being about ± 2 percent from a faired mean.

Summary of Supersonic Data

Most of the available data in the Mach and Reynolds numbers range of interest come from tests in wind-tunnel facilities. At lower Reynolds numbers, they come exclusively from one such facility at Berkeley. Except for some disagreement at the lower Mach numbers between Reynolds numbers 4×10^2 and 10^3 with other wind-tunnel measurements, the data obtained by Aroesty, reference (19), seem to satisfactorily represent the drag coefficient of sphere at supersonic Mach numbers. In the region of discrepancy, the available ballistics range data seem to support those of Aroesty, so that one may conclude that Aroesty's data should be used throughout. To increase confidence, it would be highly desirable to have data generated in a facility other than a wind tunnel, specifically, a ballistics range. A technique to obtain drag data at low Reynolds numbers in a ballistics range has been developed and demonstrated by Bailey and Koch, reference (26). This involves manufacturing models out of very low-density materials, in this case, foamed plastics that are strong enough to withstand the accelerations in the gun during the launch, causing changes in the shape of the model or other of its physical constants.

DRAG TABLE

Analysis of Existing Drag Table

It is interesting to take a drag table that is presently used in reducing the falling sphere data to atmospheric densities and compare it with the drag data that has been collected and discussed in the previous sections of this report. A popular program in use is that due to Luers and Engler, reference (27). Figure 12 is a reproduction of a figure from reference (27) and shows a drag table generated utilizing Goin and Lawrence, reference (11), in the subsonic regime and Heinrich, et al, reference (16), in the supersonic regime. In Figures 13 through 15, three curves representing high, medium, and low Reynolds numbers are reproduced from Figure 12 and compared with the measured data points from the references discussed earlier. The symbols used in these figures are the same as the ones used earlier. The flagged symbols represent interpolated values in cases where actual data points in the specified narrow Reynolds number range do not exist, but can be interpolated with a fair degree of confidence. It can be seen that the drag table curves indeed follow the data of references (16) and (11) so that the accuracy of the drag table really depends on the accuracy and validity of the data in these references. As was pointed out in conclusions in the section on subsonic data, the Goin and Lawrence measurements in a ballistics range are probably the best in the subsonic regime. The drag table curves follow these data very well at all three Reynolds numbers chosen here for comparison purposes. Supersonically, as indicated by Luers and Engler, the Heinrich, et al, data were favored. As was pointed out in earlier sections, this probably was not the best of choices. These data do not agree with other measurements, especially at low Reynolds numbers. The peaks in the drag coefficient at M = 1.5 and at low Reynolds numbers in Figure 12 are solely due to one set of measurements, those of Heinrich, et al, reference (16). If the data from the Berkeley Low Density Wind Tunnel are considered, references (19), (20), (21), and (22), then one would not conclude that such a large increase in drag exists at Mach number approximately 1.5. Additional measurements between Mach numbers 1 and 2 are highly desired to define the drag coefficient in this region.

Recommended Drag Table

Based on the available drag data in the open literature, a drag table is recommended as shown in Figure 16. The drag coefficient is plotted as a function of Mach number for constant values of Reynolds number, as was done in Figure 12. The portion of the curves shown by solid lines is well substantiated by experimental data, while over the region shown by a dashed line, either measurements have not been made or the presently available data are contradictory. At subsonic Mach numbers, the data due to Goin and Lawrence, reference (11), were utilized and, therefore, this section of the plot is identical to Figure 12. Supersonically,

the Aroesty, reference (19), Wegener and Ashkenas, reference (25), May, reference (23), and May and Witt, reference (23), measurements were considered foremost, and, therefore, the curves are considerably different from those in Figure 12. The notable difference in the presently recommended drag table is the absence of the peak in drag coefficient at Mach number approximately 1.5. The measurements utilized for this table showed very little or no effect of Mach number in the supersonic regime. To increase its usefulness, the recommended drag curves of Figure 16 are tabulated in Table I.

Recommended Future Tests

In Figure 1, the ranges of interest in Mach and Reynolds numbers in the atmospheric sensing experiments are shown. This figure is reproduced in Figure 17, in which the area shown by the fine cross hatching represents Mach and Reynolds numbers for which experimental data are available and the drag coefficient of spheres can be predicted with confidence. Outside this, additional tests would be desirable. Some incompressible data at higher Reynolds numbers do exist, but there is slight disagreement among them. It would be relatively easy to extend tests like those of Goin and Lawrence, reference (11), to measure the drag coefficients there. At higher subsonic Mach numbers, there are certain Reynolds number regions where interpolation would not likely give accurate results. Ballistics range tests would be simple and relatively inexpensive to perform in this area and, therefore, are recommended. No data exist at transonic and low supersonic Mach numbers. Tests have been made between Mach numbers 1.5 and 3, mostly in wind tunnels. Considerable contradiction exists between different test results in this region while each set of data has rather large scatter or probable error. Aroesty's, reference (19), measurements are the most comprehensive and his data are recommended. At Mach numbers around 2, these data possess approximately ± 7 percent scatter, and, therefore, it would be advisable to confirm these results with additional tests in a ballistics range. A technique to obtain drag data at low Reynolds numbers has been developed by Bailey and Koch, reference (26). A ballistics range test has the advantage of having no local disturbances around the model, like wire or string supports, or disturbances in the free stream that hamper a wind-tunnel test, especially at low Reynolds numbers, where they have a marked effect on the drag.

APPLICABILITY OF GROUND TEST DATA TO FULL-SCALE FLIGHT

The models used in all the tests discussed so far have been perfect spheres, or as nearly perfect as has been possible to manufacture them. The out of roundness was checked and controlled so that it would be within certain small tolerances. The surface was usually polished to have a minimum surface roughness. In all cases, the spheres were made of solid material and can be considered undeformable under the loads experienced in the tests. In all but one investigation, which will be described later in this report,

the surface temperature of the sphere was not altered from that which normally exists during these tests. In case of the wind tunnel, the sphere reaches an equilibrium with the surrounding stream and is considered to be at the recovery temperature of the free stream. In a ballistics range, the model normally is at room temperature when it is loaded in the gun and because of the short flight duration, the total heat input during the flight is not high enough to raise its temperature.

In an atmospheric sensing experiment, on the other hand, the vehicle considered herein is an inflatable balloon for which the above-mentioned properties may not apply. These balloons are made of 0.5-mil-thick mylar cut into panels which are butt jointed and taped. Because of this, there are surface irregularities and roughness elements at the taped joints. They may be deformed due to the surrounding pressure distribution, especially at lower altitudes. Finally, the heat transfer at the wall of the balloon may not be the same as in a ground test, due to solar heating of the balloon surface.

A question that remains is how applicable are the data gathered in various testing facilities on model spheres to the atmospheric sensing balloon flights. There has been some attempt made to investigate the effect of parameters such as rotation, heat transfer, and surface roughness on the drag coefficient. These will be discussed in the following sections of this report.

Effect of Rotation

The rocket carrying the tightly packed mylar balloon on its way up is spin stabilized. Therefore, it can be expected that after ejection the inflated sphere will be rotating as well. The spin rate of the dart prior to ejection is between 25 and 30 rps. After the sphere is deployed and fully inflated, the rotational velocity will decrease considerably because of the increase in moment of inertia. To estimate the rotational velocity of the balloon, let us apply the law of conservation of angular momentum to the system consisting of the balloon material. It is assumed here that the isopentane gas and the aluminum capsule containing it have a negligible effect on the moment of inertia of the system. The mylar material is assumed to be homogeneously distributed in a cylinder inside the staves in the initial position and in the walls of the sphere in the final position. Conservation of angular momentum requires that

$$(I\omega)_{cyl} = (I\omega)_{sphere} = \text{Constant}$$

$$\frac{1}{2} m r_{cyl}^2 = \frac{2}{5} m \frac{r_o^5 - r_i^5}{r_o^3 - r_i^3} \omega_f$$

where r_o is the outside radius and r_i is the inside radius of the sphere. Solving for ω_f/ω_i and gets

$$\frac{\omega_f}{\omega_i} = \frac{5}{4} r_{cyl}^2 \frac{r_o^3 - r_i^3}{r_o^5 - r_i^5}$$

Introducing $t = r_o - r_i$ and expanding

$$\frac{\omega_f}{\omega_i} = \frac{5}{4} r_{cyl}^2 \frac{r_o^3 - r_o^3 + 3 r_o^2 t - 3 r_o t^2 + t^3}{r_o^5 - r_o^5 - 5 r_o^4 t - 10 r_o^3 t^2 + 10 r_o^2 t^3 - 5 r_o t^4 + t^5}$$

$$\frac{\omega_f}{\omega_i} = \frac{5}{4} r_{cyl}^2 \frac{r_o^2 t \left[3 - 3 \left(\frac{t}{r_o}\right) + \left(\frac{t}{r_o}\right)^2\right]}{r_o^4 t \left[5 - 10 \left(\frac{t}{r_o}\right) + 10 \left(\frac{t}{r_o}\right)^2 - 5 \left(\frac{t}{r_o}\right)^3 + \left(\frac{t}{r_o}\right)^4\right]}$$

$$\frac{\omega_f}{\omega_i} = \frac{5}{4} \frac{r_{cyl}^2}{r_o^2} \left[\frac{3 - 3\epsilon + \epsilon^2}{5 - 10\epsilon + 10\epsilon^2 - 5\epsilon^3 + \epsilon^4}\right]$$

where

$$\epsilon = \frac{t}{r_o} = \frac{.0005"}{19.7"}$$

Since the thickness of mylar is very small compared to the sphere diameter, all terms involving ϵ may be neglected compared to the constants inside the brackets. Therefore,

$$\frac{\omega_f}{\omega_i} = \frac{3}{4} \left(\frac{r_{cyl}}{r_o}\right)^2$$

For r_{cyl} = 1/2 inch and r_o = 19.7 inches

$$\frac{\omega_f}{\omega_i} = .000483$$

$$\omega_f = .000483 \times 30 = .01449 \text{ rev/sec} = 5.22 \text{ deg/sec}$$

There is only one work in which the effect of sphere rotation was specifically measured in a wind-tunnel test. This was reported in reference (16). Figure 18 is a reproduction of a figure from the above reference. Although the Reynolds numbers in these tests were above those of interest in the falling sphere experiments, they may indicate qualitatively a trend at lower Reynolds numbers as well. The measurements were made at low velocities, certainly in the incompressible regime. In Figure 18, the drag coefficient is plotted against the ratio of the circumferential and free-stream velocities, $\omega r/V$. It can be seen that C_D does vary with the velocity ratio but that for small spin rates, i.e., for values of $\omega r/V$ less than 0.2, it appears to be constant. It is very unlikely that such high spin rates will ever be experienced by the falling balloons. As was seen, the spin rate resulting from the dart rotation is very low. Furthermore, the fall velocity at the high altitudes will be high, resulting in negligibly small velocity ratios, $\omega r/V$. At low altitudes, the roughnesses and irregularities in the balloon surface could induce some rotation, but, here again, the values of spin rates will be small compared to the fall velocity. Unless there is a drastically different effect of rotation on drag at low Reynolds numbers and higher Mach numbers than that shown in Figure 18, it can be concluded that the amount of rotation that the falling sphere may experience has negligible effect on its drag coefficient.

Effect of Surface Temperature

It has been found that reducing the surface temperature of the sphere in a wind-tunnel test that is increasing the heat transfer at the wall at supersonic Mach numbers reduces the drag coefficient. This has been reported by Aroesty, reference (19). In this investigation, the sphere temperature was reduced to 80 degrees K in a reservoir above the edge of the wind-tunnel jet, and the sphere was permitted to fall into the jet, where its trajectory was recorded by high-speed motion picture camera. As in a ballistics range test, the duration of the test is so short that it is assumed that the sphere temperature does not change during the test.

The measurements at about Mach number 2 are presented in Figure 19, which is a reproduction of a figure from reference (19). Here, drag coefficient is plotted against Reynolds number based on gas properties behind a normal shock. Data points for the adiabatic wall case have been omitted; only the fitted regression curve has been reproduced as a solid line. This is the same curve as was shown in Figure 9. The cold wall data points are shown as open circles and a line faired through these data. It is seen that a severe cooling of the wall from 300 degrees K to 80 degrees K reduces the drag coefficient at the lower Reynolds number range by about nine percent. At higher Reynolds numbers, the cold wall data seem to fair into the adiabatic data.

In Figures 20 and 21, the cold wall data are compared to the regression curves fitted to the adiabatic data at Mach numbers near

4 and 6, respectively. Here again, the drag coefficient is plotted against Reynolds number based on properties behind the normal shock. Although the scatter in these data is quite large, it can be concluded that there is a marked decrease in the drag coefficient as the temperature of the sphere is decreased.

The spheres in these tests were subjected to very severe cooling conditions. The temperature of the sphere was lowered from room temperature of approximately 300 degrees K to about 80 degrees K. This was accompanied by a reduction in drag coefficient of as much as ten percent from the standard incompressible curve values. During a balloon flight, on the other hand, cooling of its surface below the equilibrium temperature cannot occur. In fact, heating of the surface mainly from solar radiation is expected. There has been one test conducted on heated spheres at Mach number near 4 and in the Reynolds number range $30 < Re_2 < 50$, reference (28). The sphere temperature was raised so that the wall-to-stagnation temperature ratio was 2.6 and about ten percent increase in drag coefficient resulted. The data points are shown by an open square symbol (□) in Figure 20. It is impossible for the mylar material in the balloon to sustain such large temperature increases. Therefore, only a very small rise in the drag coefficient can be expected at supersonic Mach numbers as the balloon gets heated from the sun.

The effect of surface temperature on drag coefficient at subsonic Mach numbers and under incompressible conditions is not known. In these regimes, what governs the drag coefficient is the contribution from the base drag, which, in turn, is dependent on the location of flow separation on the body. As the balloon surface is heated by radiation from the sun and the surroundings, the boundary layer may be stabilized and, therefore, retard separation. This effect is not known, and a detailed study of this problem is recommended.

Effect of Surface Roughness

Unlike the sphere models used in the many tests described earlier in this report that generally had polished surfaces, the inflated spherical balloon in flight will have some roughness on its surface. The mylar balloon is folded and squeezed between a set of cylindrical staves that fit inside the dart used for launching. It may be left in this tightly packed configuration for some time before it is launched, during which wrinkles set into the mylar. After it is inflated, the mylar may not be the smooth material that it was at the time of manufacture, but contains tiny fold marks all over it. Any roughness elements will probably be small compared to boundary-layer thickness. Another source of roughness is the seams. Here, the mylar material is butt joined and secured with heat-sensitive tape. This could be a significant source of roughness, since the wrinkles in these seams are quite pronounced. There also is some dimpling in the panels where the

radar reflective material is attached to the interior of the wall. This should be considered more like a surface irregularity rather than roughness. It could affect the point of separation of the boundary layer and, therefore, drag.

There have been some tests performed on spheres with surface roughness. Roughened spheres were launched in a ballistics range at supersonic Mach numbers, although at Reynolds numbers higher than a falling balloon would experience. The results are reported by Charters and Thomas in reference (29) and are reproduced in Figure 22. The solid line represents data on smooth spheres generated during the same investigation. The models used were smooth ball bearings. The three data points (Δ) in Figure 22 were obtained with a rough sphere. In this case, a 9/16-inch-diameter ball bearing was annealed, and a criss-cross pattern of 1/16-inch-deep grooves were filled over the surface about 1/8 inch apart. Only a slight increase, about three percent, in drag coefficient was measured over the smooth sphere value.

In the incompressible regime and at low Reynolds numbers, a study of the effect of roughness or drag was performed by Sivier, reference (30). It was found that rather large roughness elements have to be applied to the sphere in order to have a measurable effect on drag. The largest roughness factor, k (ratio of roughness height to sphere diameter), in those tests was 0.175. Below Reynolds number 500, the rough sphere drag coefficients were a very small amount below those for the smooth sphere; while for Reynolds number above 500, rough sphere C_D increased systematically with increasing roughness factor, k. Very large increases in drag coefficient with roughness were measured by Selberg, reference (31), in Reynolds number region between 600 and 1700, also at very low Mach numbers. Three types of balls were tested in a shocktube, each representing different roughnesses. Although no measurements of k were made, the ball materials were sapphire, gunpowder, and glass and were classified as smooth, rough, and very rough, respectively. The results from reference (31) are reproduced in Figure 23. There is considerable scatter among the data which can be attributed to the random roughness elements and their random distribution over the surface. The balls may not have been perfect spheres to begin with. These results indicate that, indeed, the roughness of the surface at Reynolds numbers representative of those experienced by the atmospheric sensing balloons at low Mach numbers affect the drag coefficient considerably. Although the size of the roughness elements on the mylar spheres is relatively small, compared to the roughness on Sivier's, reference (30), and Selberg's, reference (31), models, it is conceivable that the seams and the irregularities in the balloon surface could cause the drag coefficient to be slightly different from the smooth sphere curve values. The amount of correction for roughness is not known, and a detailed study of the effect should be made, specifically of the effect of roughness on the flow separation point.

CONCLUSIONS

The presently available drag data on spheres in a Reynolds-Mach number range of interest to the falling sphere technique of atmospheric sensing have been collected and analyzed. The following conclusions can be drawn from this study:

1. The incompressible curve has been well established by Wieselsberger, reference (1), and Allen, reference (3), and substantiated by recent measurements by Goin and Lawrence, reference (11). Except for Rd > 10^4, where slight discrepancies exist between the results from the two sets of measurements, this curve can be considered to represent the drag coefficient of spheres for $M \leq 0.2$.

2. At subsonic, compressible Mach numbers, the data obtained in a ballistics range by Goin and Lawrence, reference (11), are recommended. Additional measurements are desired since there are rather wide regimes of Reynolds number where measurements have not been made.

3. No experimental data on sphere drag are available in the transonic Mach number region.

4. Whatever data exist in the Mach number region from one to two are contradictory or have very large probable errors. It is highly desired to generate additional data in this region.

5. For Mach numbers between two and five, C_D can be predicted with an adequate degree of confidence. Measurements by Aroesty, reference (19), May and Witt, reference (24), and Wegener and Ashkenas, reference (25), were used to define the drag curve.

6. Rotation of the sphere is expected to be low enough not to have a measurable effect on its drag.

7. Large changes in surface temperature from that of equilibrium have produced measurable changes in C_D at supersonic Mach numbers. At low subsonic Mach numbers, the effect of surface temperature on drag is not known.

8. In the Reynolds number range of interest, large roughnesses on the surface of the sphere have produced large increases in drag, small roughnesses, correspondingly smaller changes in drag. A detailed study of roughness at low subsonic Mach numbers is recommended.

REFERENCES

(1) von C. Wieselsberger, "Weitere Feststellung über die Gesetze des Flüssigkeits-und Luftwiderstandes," Physikalische Zeitschrift, 23 Jahrgang, No. 10, pp 219-224, 15 May 1922

(2) "Versuchsergebnisse b) Der Widerstand von Kugeln, Ellipsoiden, und Scheiben," Ergebnisse der Aerodynamischen Versuchsanstalt zu Göttingen. II Lieferung, Verlag R. Oldenburg in München und Berlin, pp 28-32, 1923

(3) Allen, H. S., "The Motion of Sphere in a Viscous Fluid," Philosophical Magazine, Ser. 5, Vol. 50, p 323

(4) von C. Wieselsberger, "Mitteilung aus der Göttinger Modellversuchsanstalt, 16. Der Luftwiderstand von Kugeln," Zeitschrift für Flugtechnik und Motorluftschiffahrt, Jahrgang V, Heft 9, pp 140-145, 16 May 1914

(5) von O. Flachsbart, "Neue Untersuchungen über den Luftwiderstand von Kugeln," Physikalische Zeitschrift, No. 13, 28. Jahrgang, pp 461-469, 1 Jul 1927

(6) von O. Flachsbart, "Der Widerstand von Kugeln in der Umgebung der Kritischen Reynoldssen Zahl," Ergebenisse der Aerodynamischen Versuchsanstalt zu Göttingen, IV Lieferung, Verlag von R. Oldenburg, pp 106-108, 1932

(7) Charters, A. C., and Thomas, R. N., "The Aerodynamic Performance of Small Spheres from Subsonic to High Supersonic Velocities," Journal of the Aeronautical Sciences, pp 468-476, Oct 1945

(8) von A. Naumann, "Luftwiderstand der Kugel bei hohen Unterschallgeschwindigkeiten," Allgemeine Wärmetechnik, Zeitschrift für Wärme-und Kältetechnik, 3. Jahrgagn, pp 217-221, 1952

(9) von H. Liebster, "Über den Widerstand von Kugeln," Annalen der Physik, Vol. 82, pp 541-562, 1927

(10) Lunnon, R. G., "Fluid Resistance to Moving Spheres," Royal Society Proceedings, Ser. A, Vol. 110, pp 680-694, 1926

(11) Goin, K. L., and Lawrence, W. R., "Subsonic Drag of Spheres at Reynolds Numbers from 200 to 10,000," AIAA Journal, Vol. 6, No. 5, pp 961-962, May 1968

(12) Shakespeare, G. A., "Experiments on the Resistance of the Air to Falling Spheres," Philosophical Magazine, Vol. 28, pp 728-734, 1914

(13) Möller, von Wilhelm, "Experimentelle Untersuchungen Zur Hydrodynamik der Kugel," Physikalische Zeitschrift, No. 2, 39. Jahrgang, pp 57-80, 15 Jan 1938

(14) Schlichting, H., Boundary Layer Theory, McGraw-Hill Book Co., p 9, 1955

(15) Heinrich, Helmut G., "Aerodynamic Drag Characteristics of Spherical Balloons (Robin) Descending from 70 km Altitude," University of Minnesota, Institute of Technology, Dept. of Aeronautics and Engineering Mechanics, Minneapolis, Minn., 1964

(16) Heinrich, H. G., Niccum, R. J., Haak, E. L., Jamison, L. R., and George, R. L., "Modification of the Robin Meteorological Balloon, Volume II - Drag Evaluations," Dept. of Aeronautics and Engineering Mechanics, University of Minnesota, Contract No. AF 19(628)-2945, Project No. 6670, Task No. 667004, 30 Sep 1965
(17) Heinrich, H. G., and Noreen, R. A., "An Assessment of Sphere Drag Coefficient Data," Status of Passive Inflatable Falling-Sphere Technology for Atmospheric Sensing to 100 km, Symposium held at Langley Research Center, Hampton, Va., NASA SP-219, pp 93-110, Sep 1969
(18) Zarin, N. A., "Measurement of Non-continuum and Turbulence Effects on Subsonic Sphere Drag," NASA CR-1585, Jun 1970
(19) Aroesty, J., "Sphere Drag in a Low Density Supersonic Flow," University of California, Institute of Engineering Research, Berkeley, Calif., Technical Report HE-150-192, 3 Jan 1961
(20) Kane, E. D., "Drag Forces on Spheres in Low Density Supersonic Gas Flow," University of California, Department of Engineering, Berkeley, Calif., Technical Report HE-150-65, 15 Feb 1950
(21) Kane, E. D., "Sphere Drag Data at Supersonic Speeds and Low Reynolds Numbers," Journal of the Aeronautical Sciences, Apr 1951
(22) Sherman, Frederick S., "Note on Sphere Drag Data," Journal of the Aeronautical Sciences, Aug 1951
(23) May, A., "Supersonic Drag of Spheres at Low Reynolds Numbers in Free Flight," NOL NAVORD Report 4392, 1957
(24) May, A., and Witt, W. R., "Free-Flight Determinations of the Drag Coefficients of Spheres," Journal of the Aeronautical Sciences, Vol. 20, No. 9, Sep 1953
(25) Wegener, P. P., and Ashkenas, H., "Wind-Tunnel Measurements of Sphere Drag at Supersonic Speeds at Low Reynolds Numbers," Journal of Fluid Mechanics, Vol. 10, 1961
(26) Bailey, A. B., and Koch, K. E., "Launching of Foamed Plastic Models with a Two-Stage Light Gas Gun," AEDC-TR-66-60, May 1966
(27) Luers, J., and Engler, N. A., "High-Altitude Robin Data-Reduction Program," NASA SP-219, p 129, Sep 1969
(28) Chahine, M. T., "Similarity Solution for Stagnation Point Heat Transfer in Low Density, High Speed Flow," JPL, Cal Tech Research Summary 36-8, Sec. VII, 1 May 1961
(29) Charters, A. C., and Thomas, R. N., "The Aerodynamic Performance of Small Spheres from Subsonic to High Supersonic Velocities," Journal of the Aeronautical Sciences, pp 468-476, Oct 1945
(30) Sivier, K. R., "Subsonic Sphere Drag Measurements at Intermediate Reynolds Numbers," University of Michigan PhD Thesis, University Microfilms, Inc., Ann Arbor, Mich., 1967
(31) Selberg, B. P., "Shock Tube Determination of the Drag Coefficient of Small Spherical Particles, NASA CR-418, Apr 1966

TABLE I

RECOMMENDED DRAG TABLE FOR SPHERES

Drag Coefficients for Various Mach and Reynolds Numbers

M \ R_e	200	600	1000	4000	10000
.1	.745	.527	.455	.388	.402
.2	.747	.531	.462	.410	.410
.3	.750	.540	.470	.403	.418
.4	.761	.554	.483	.420	.429
.5	.775	.572	.500	.440	.440
.6	.805	.601	.525	.465	.455
.7	.905	.643	.562	.510	.478
.8	1.100	.721	.622	.568	.523
.9	1.200	.850	.730	.650	.585
1.0	1.255	1.040	.928	.800	.710
1.1	1.277	1.086	1.008	.915	.857
1.2	1.292	1.105	1.028	.967	.927
1.3	1.302	1.113	1.037	.988	.950
1.4	1.312	1.222	1.047	.998	.959
1.6	1.321	1.138	1.058	1.000	.962
1.8	1.330	1.152	1.070	1.000	.971
2.0	1.334	1.169	1.080	1.002	.978
2.2	1.335	1.179	1.088	1.005	.981
2.4	1.340	1.190	1.098	1.012	.988
2.6	1.344	1.202	1.110	1.021	.994
2.8	1.348	1.212	1.119	1.029	1.000
3.0	1.352	1.222	1.130	1.040	1.008
3.2	1.357	1.232	1.140	1.050	1.015
3.4	1.360	1.241	1.150	1.060	1.021
3.6	1.362	1.250	1.160	1.070	1.028
3.8	1.365	1.260	1.171	1.081	1.034
4.0	1.365	1.267	1.180	1.092	1.040

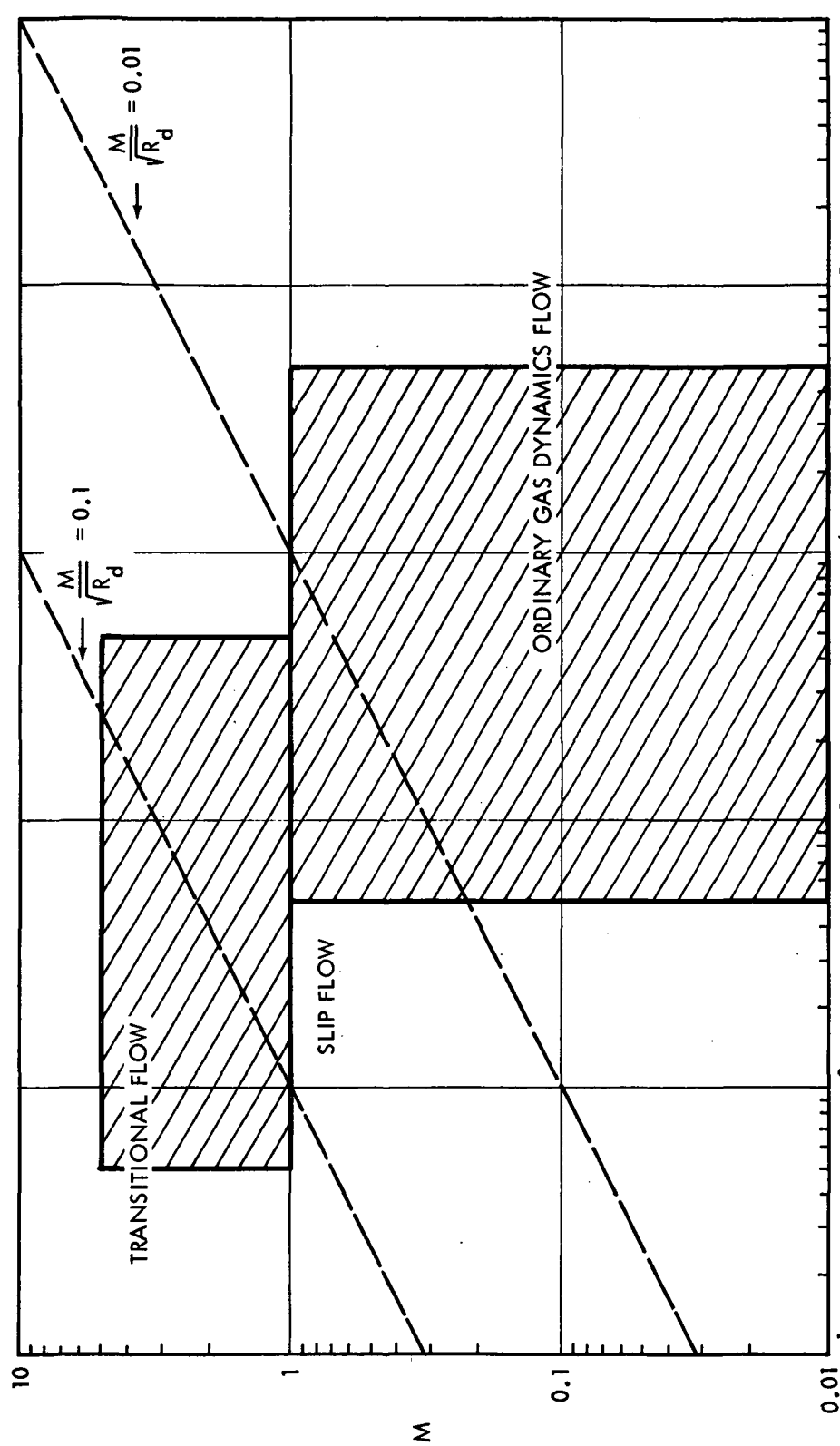

FIG. 1 RANGES OF INTEREST IN MACH NUMBER AND REYNOLDS NUMBER IN THE FALLING SPHERE TECHNIQUE OF ATMOSPHERIC SENSING

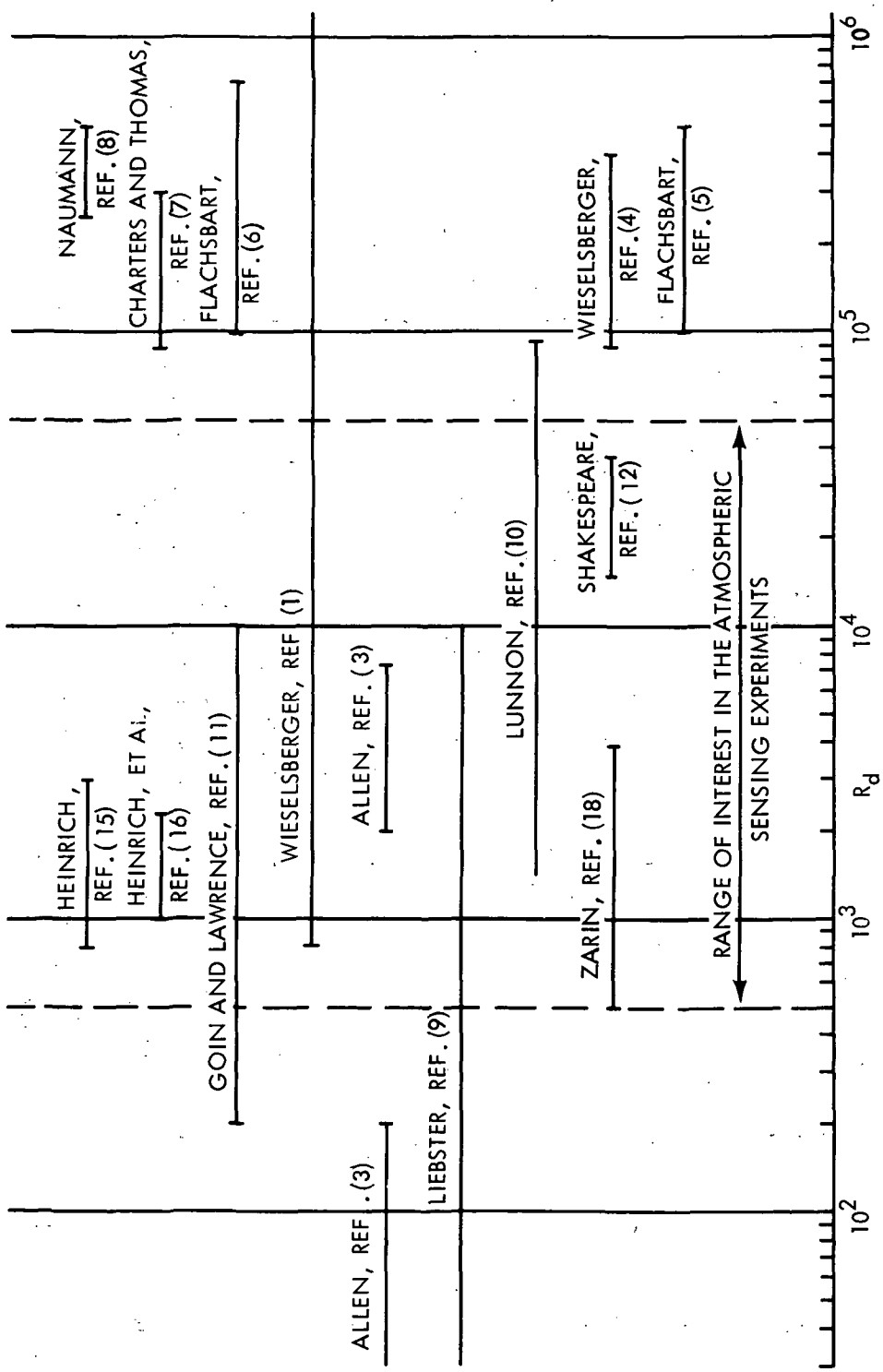

FIG. 2 REFERENCES ON SPHERE DRAG IN SUBSONIC FLOW AND THE REYNOLDS NUMBER COVERED

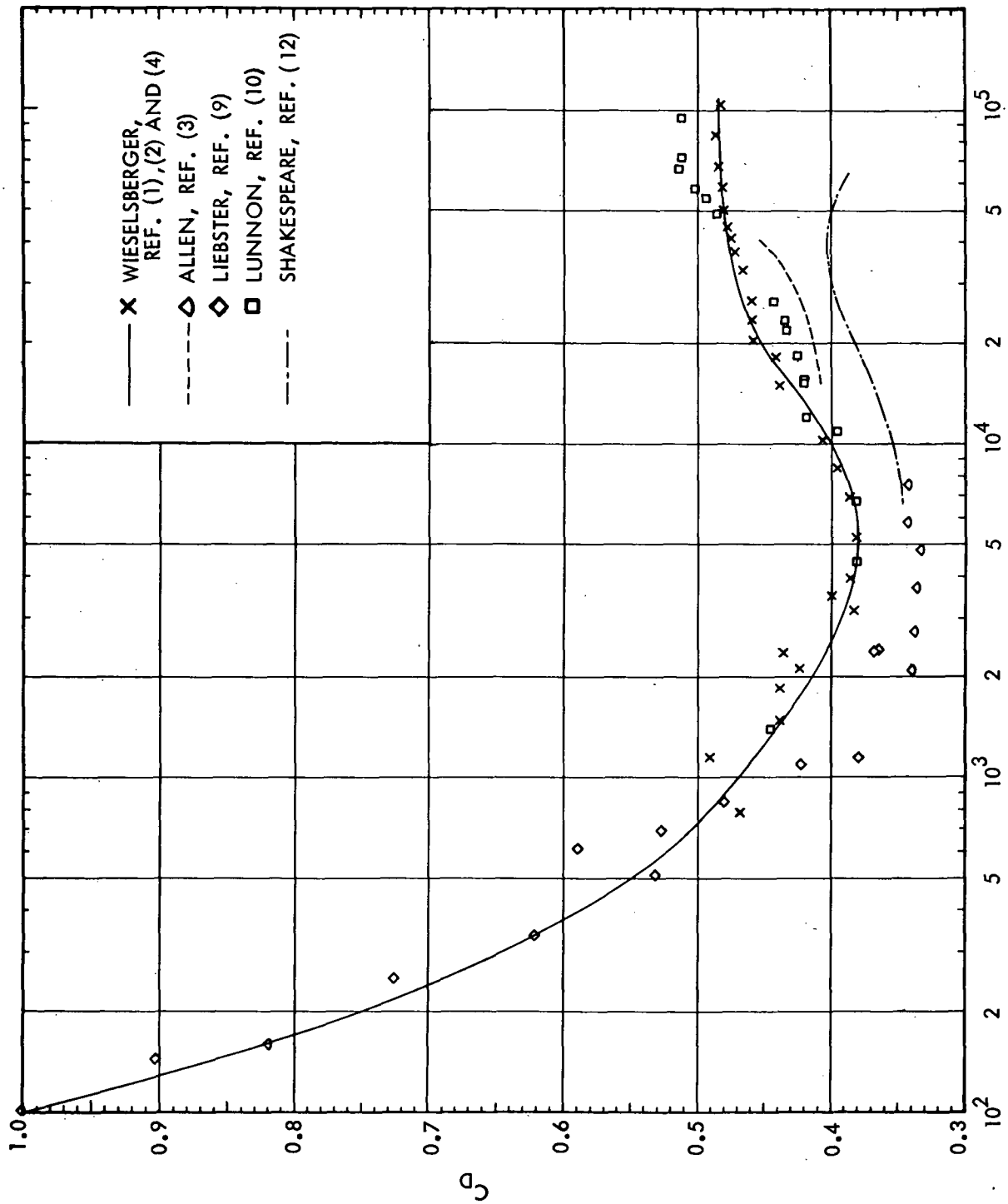

FIG. 3 DRAG COEFFICIENT OF SPHERES IN INCOMPRESSIBLE, SUBSONIC FLOW

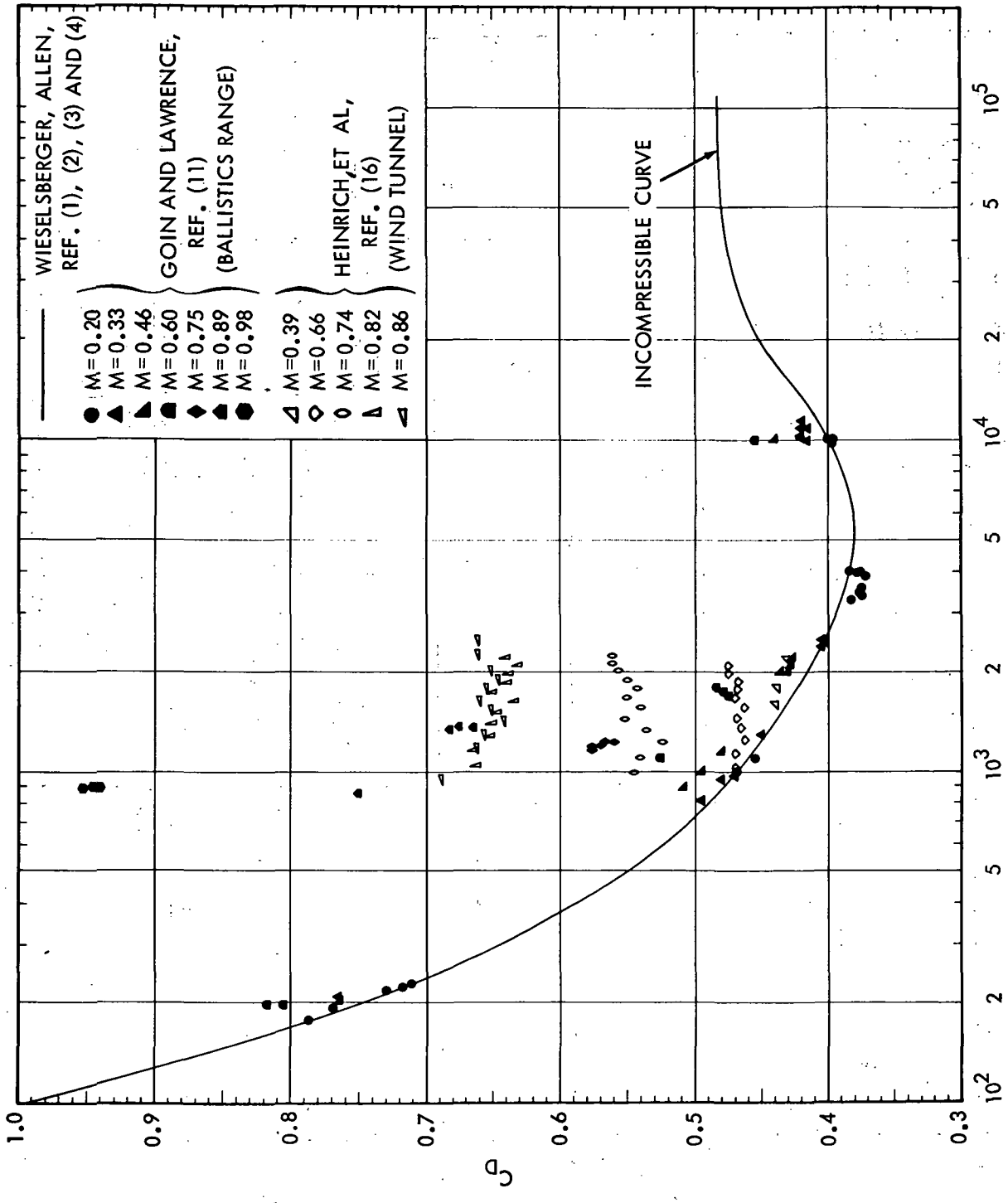

FIG. 4 DRAG COEFFICIENT OF SPHERES IN COMPRESSIBLE, SUBSONIC FLOW

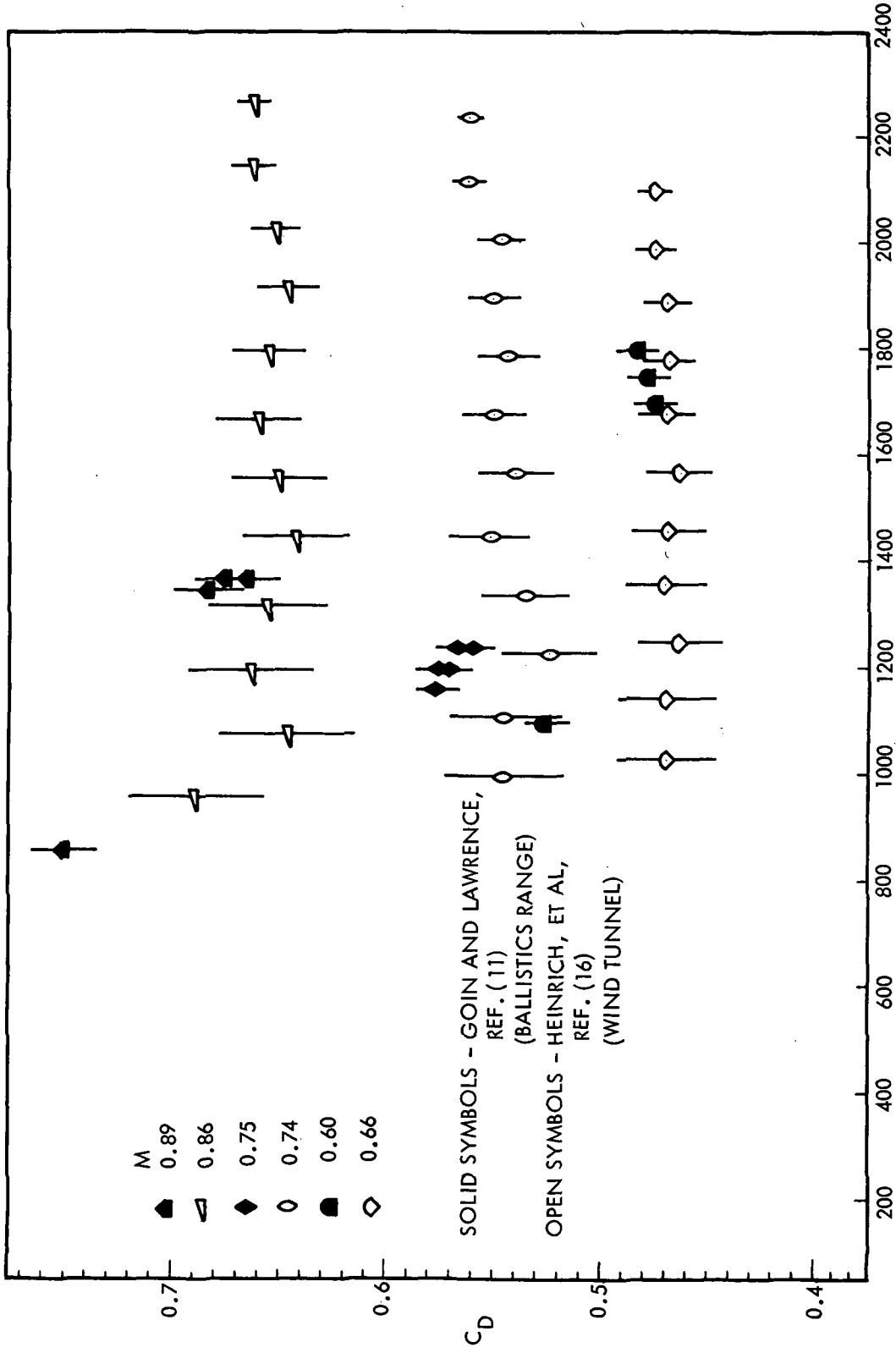

FIG. 5 COMPARISON OF SPHERE DRAG BETWEEN DATA OBTAINED IN A WIND TUNNEL AND A BALLISTICS RANGE

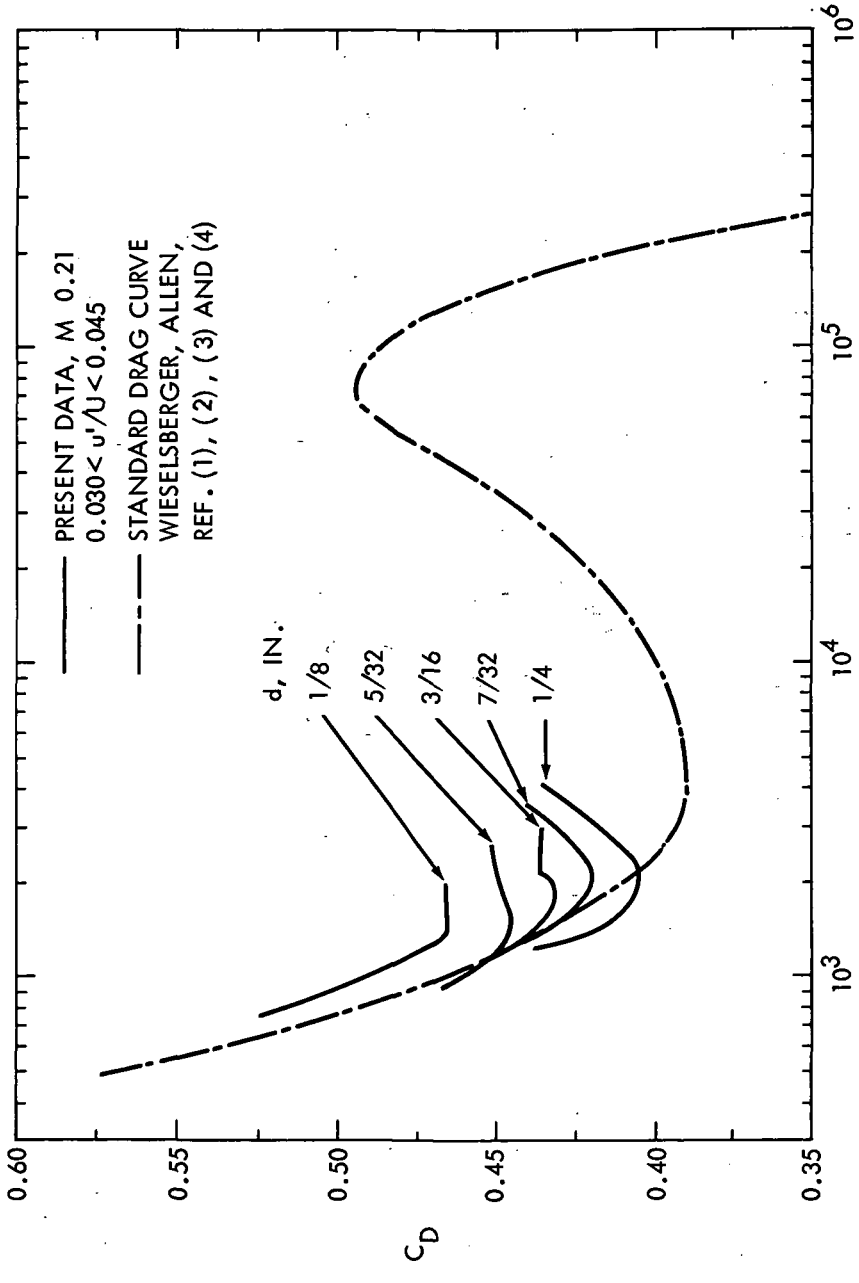

FIG. 6 DRAG COEFFICIENT OF SPHERES IN TURBULENT FLOW; M≃0.21, .030 < u'/U < .045, (ZARIN, REF.18)

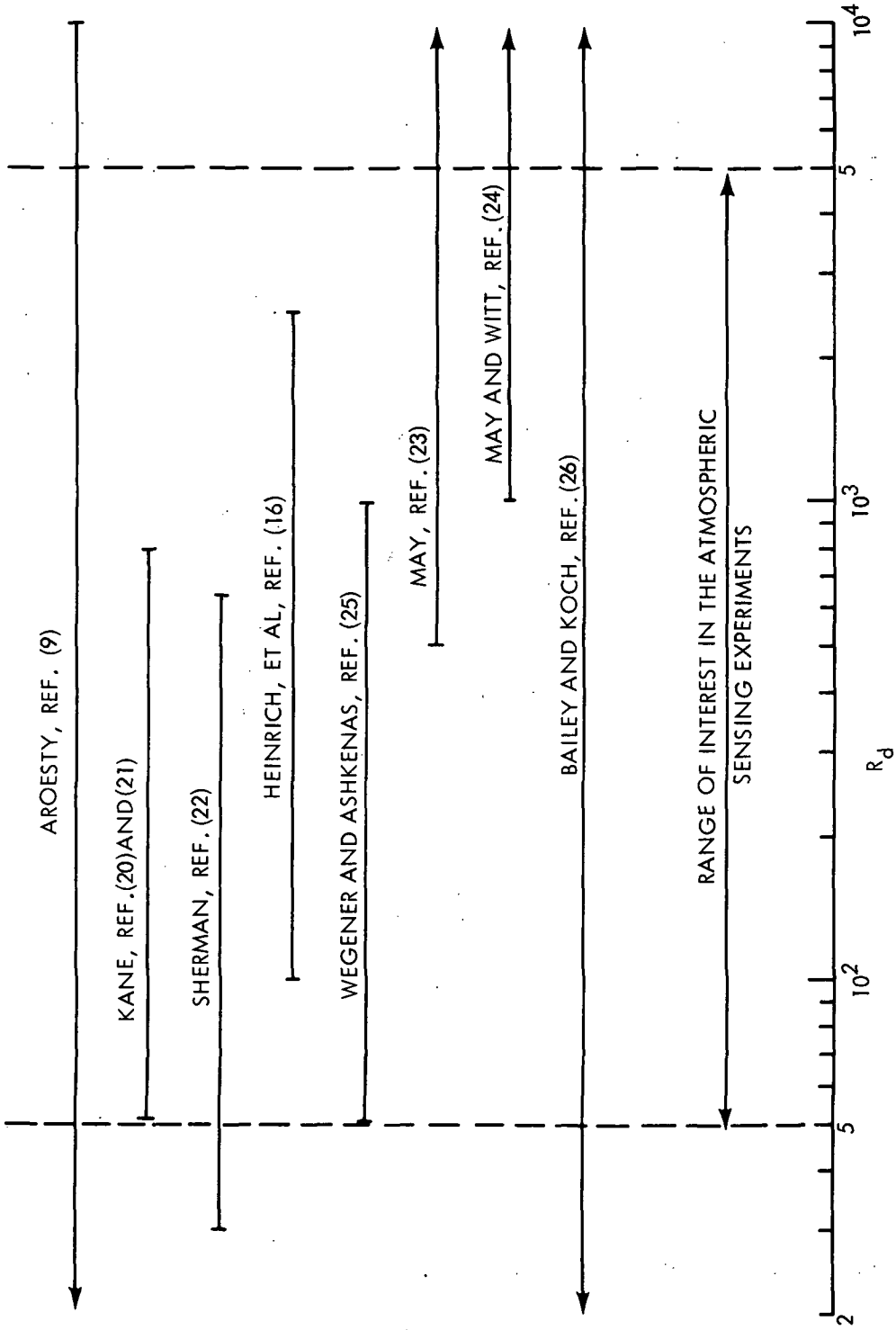

FIG. 7 REFERENCES ON SPHERE DRAG IN SUPERSONIC FLOW SHOWING THE REYNOLDS NUMBERS COVERED

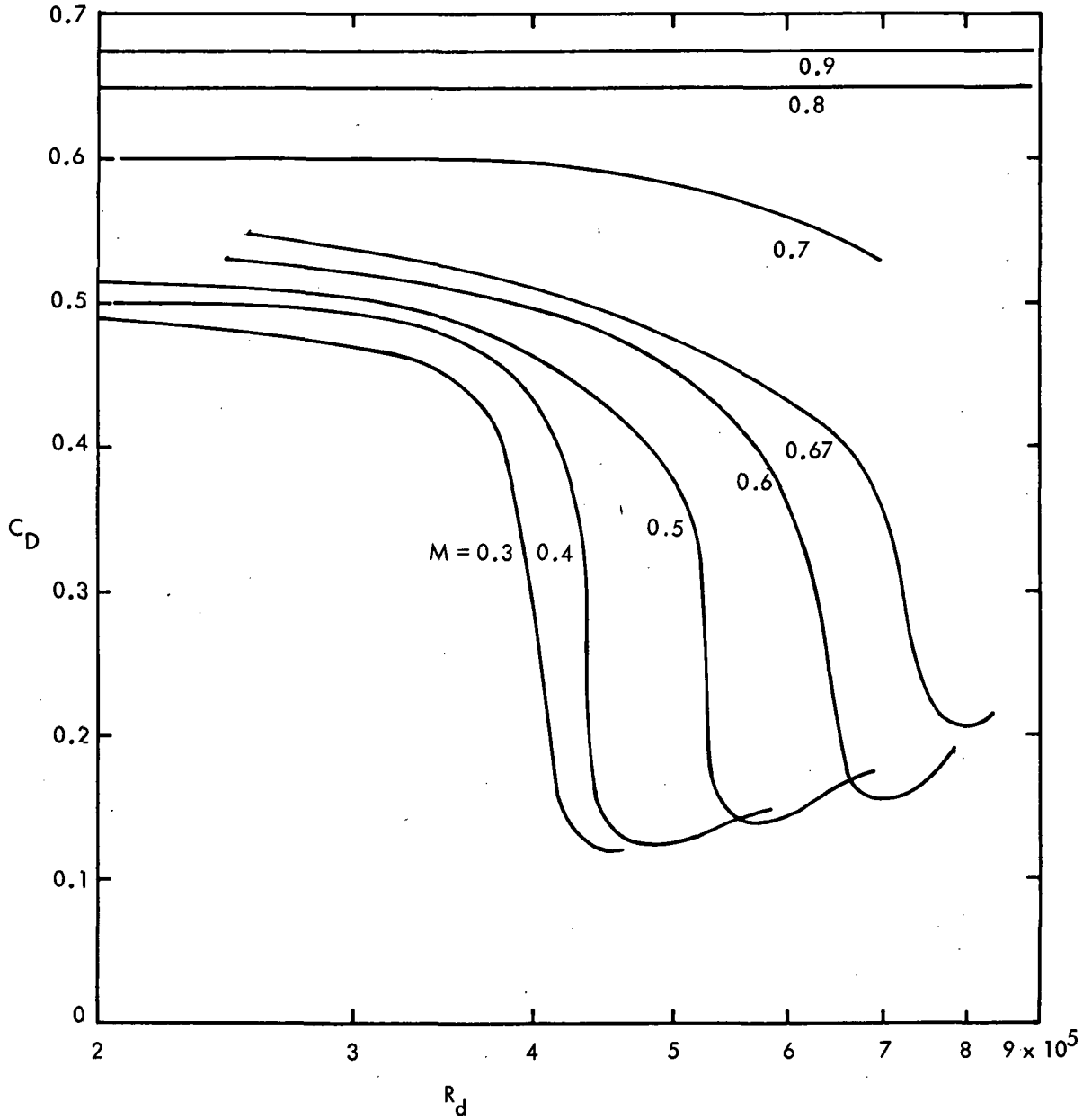

FIG. 8 DRAG COEFFICIENT OF SPHERES AS A FUNCTION OF REYNOLDS NUMBER AND MACH NUMBER IN THE REGION $2 \times 10^5 < R_d < 9 \times 10^5$, (NAUMANN, REF. (8))

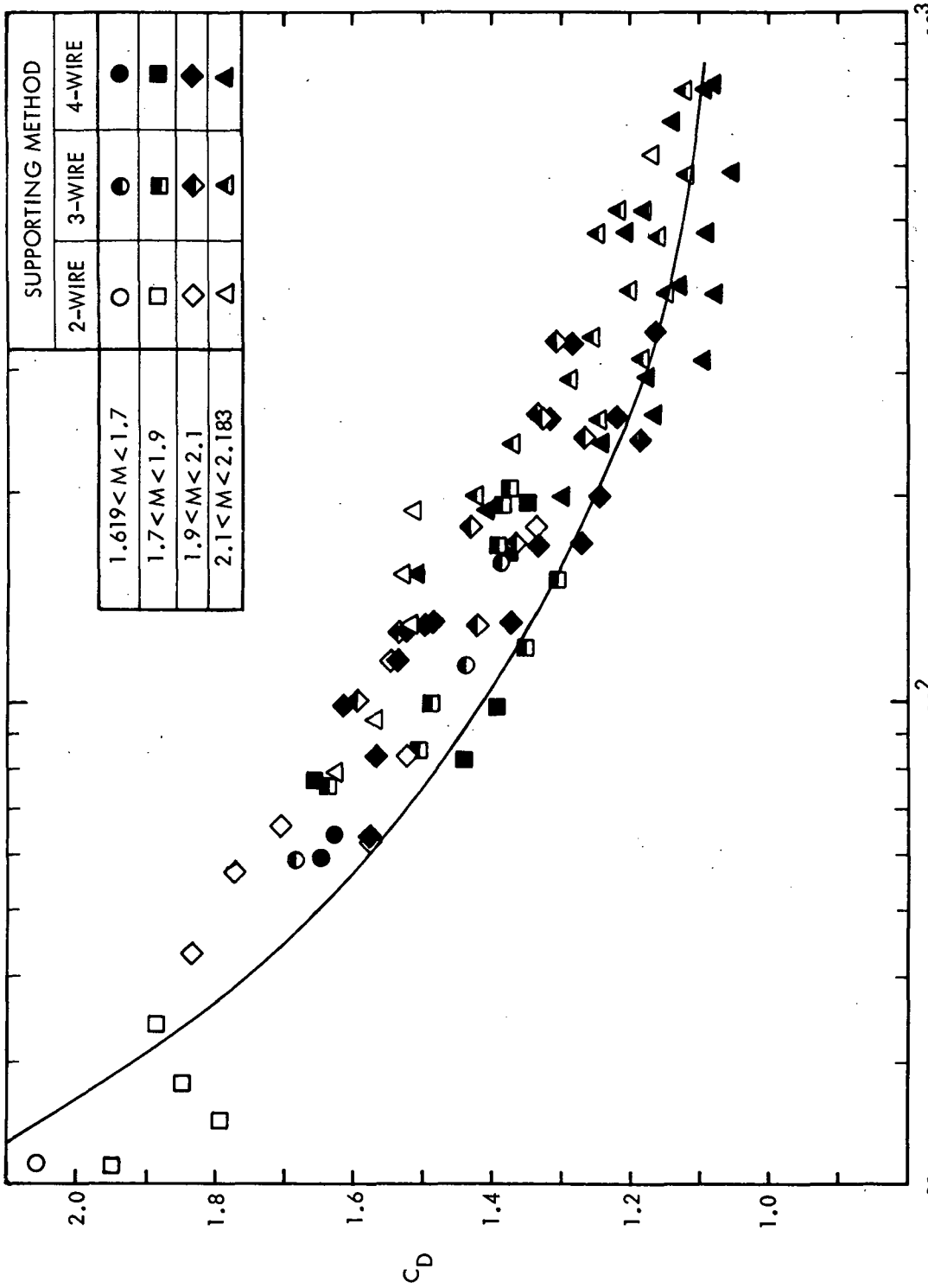

FIG. 9 DRAG COEFFICIENT OF SPHERES NEAR MACH NUMBER 2, (AROESTY, REF. (19))

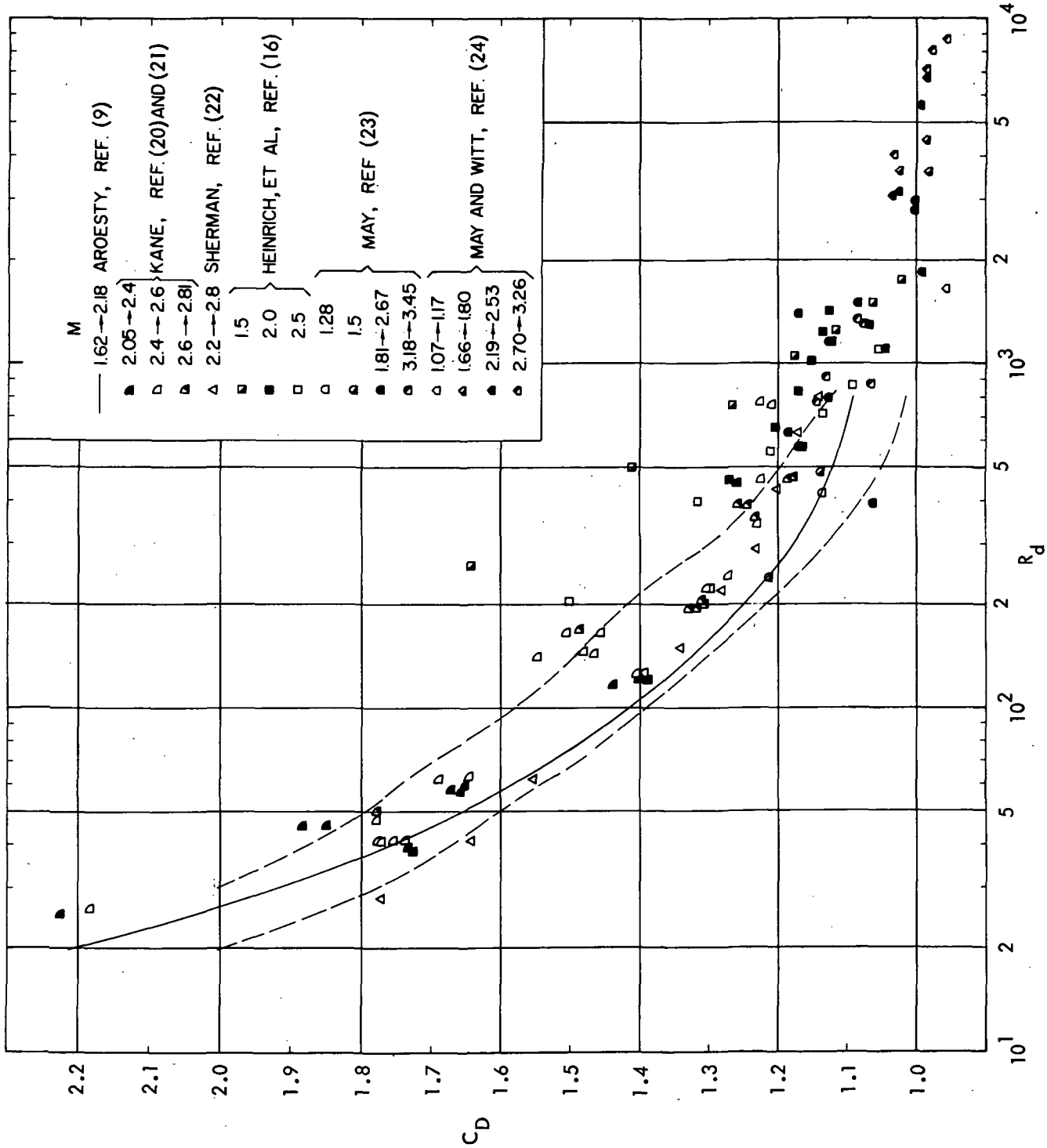

FIG. 10 DRAG COEFFICIENT OF SPHERES IN SUPERSONIC FLOW

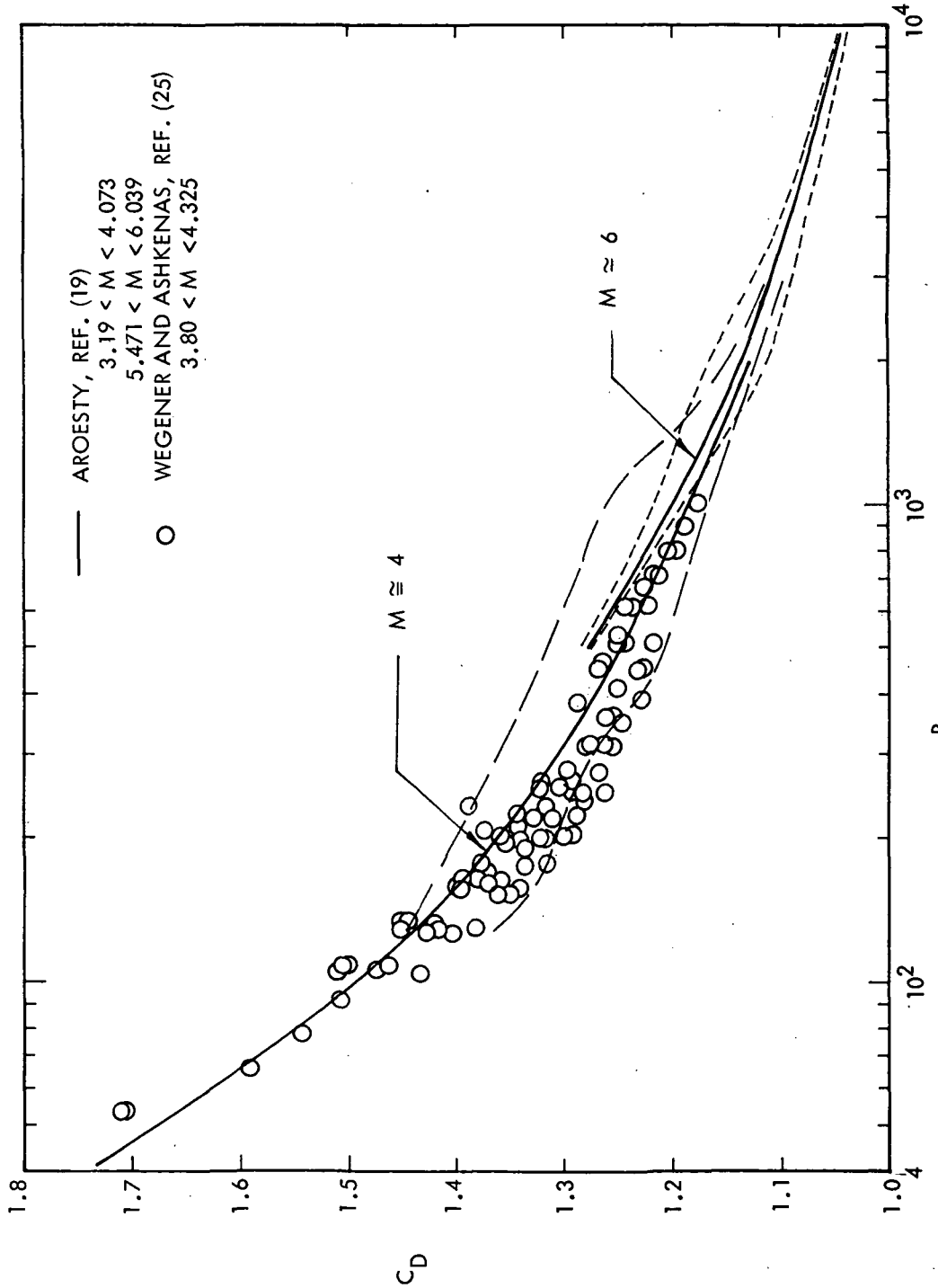

FIG. 11 DRAG COEFFICIENT OF SPHERES NEAR MACH NUMBERS 4 AND 6

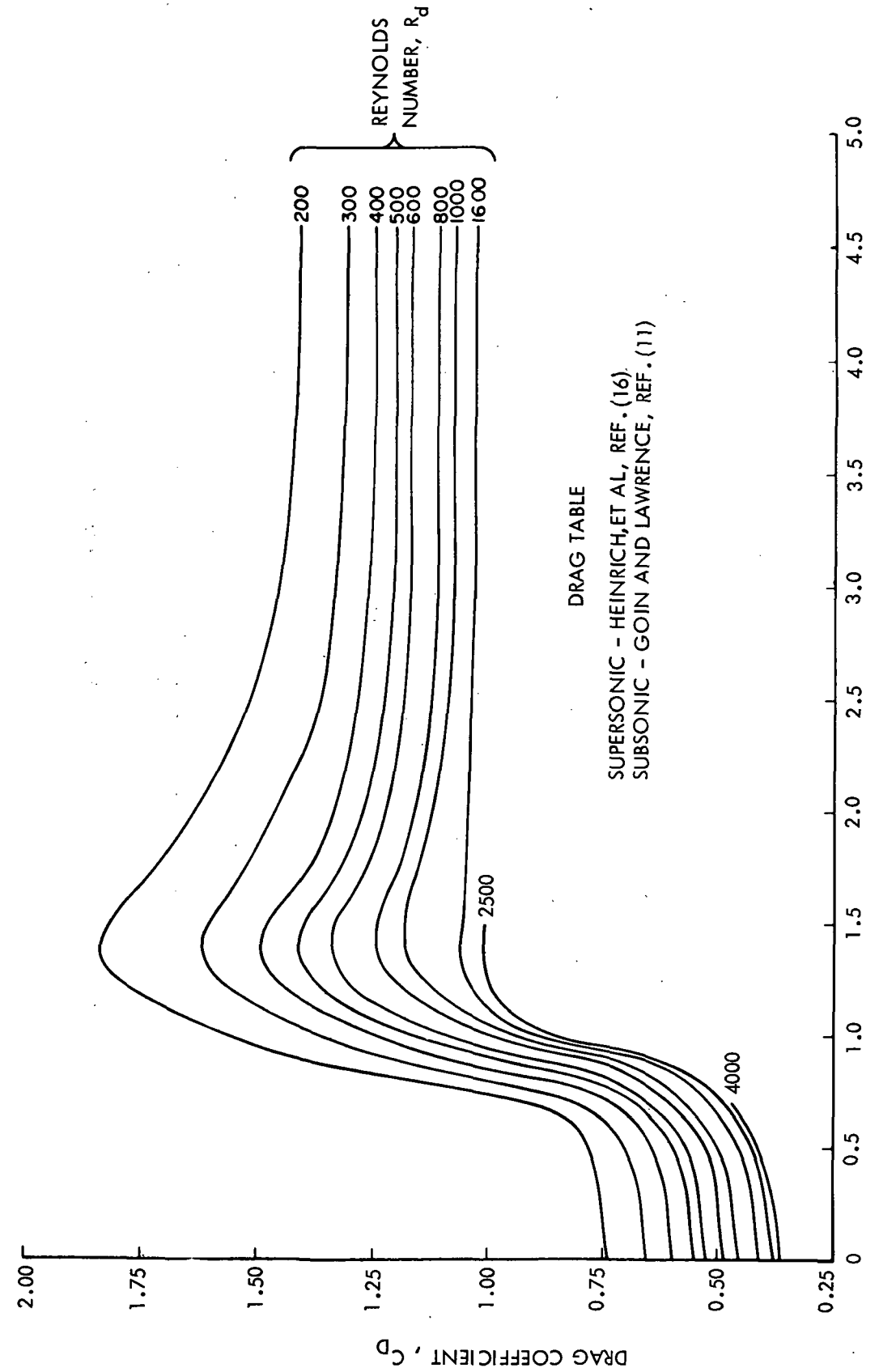

FIG. 12 SPHERE DRAG TABLE FROM LUERS AND ENGLER, REF. (27)

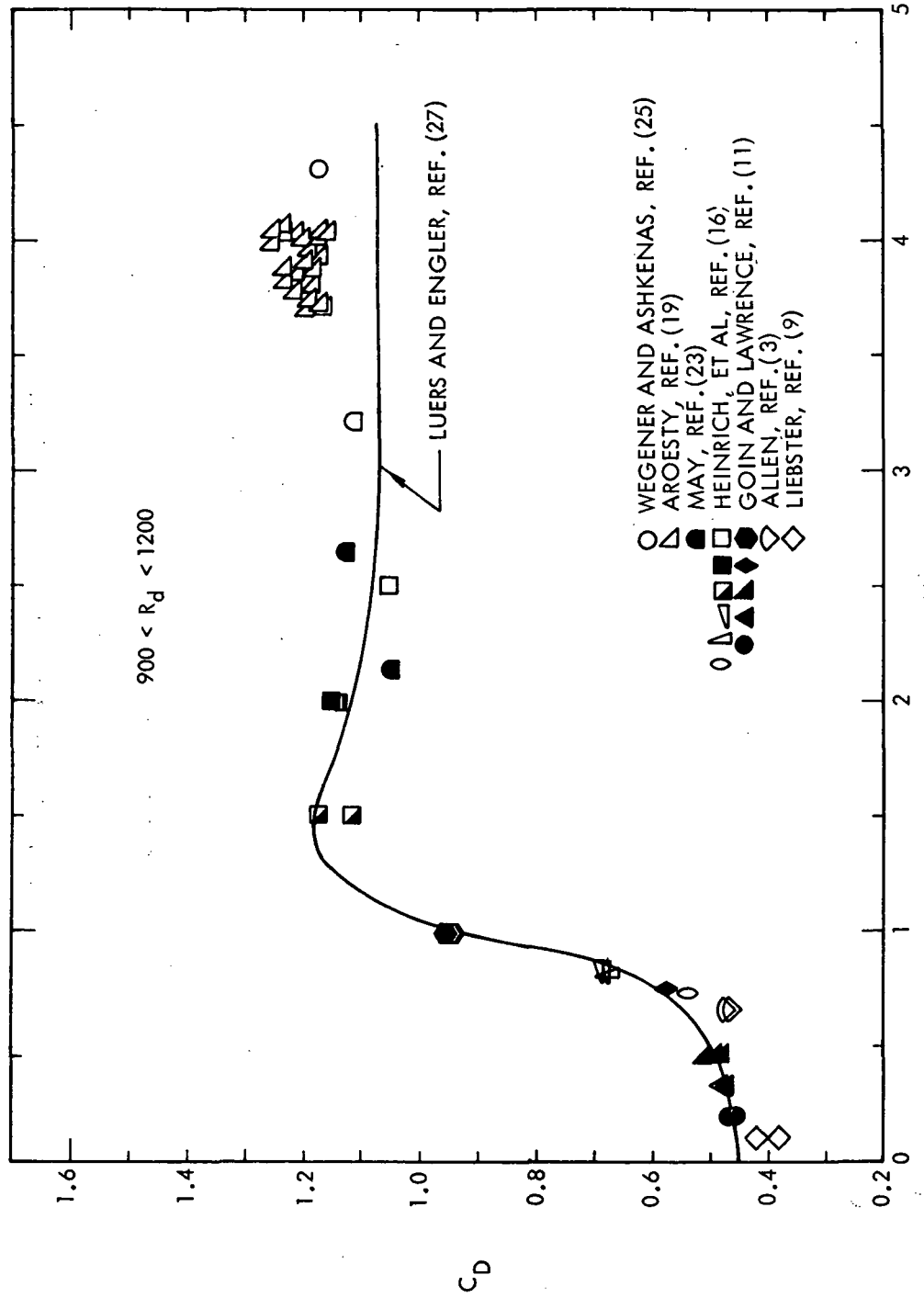

FIG. 13 DRAG COEFFICIENT OF SPHERES NEAR REYNOLDS NUMBER 10^3

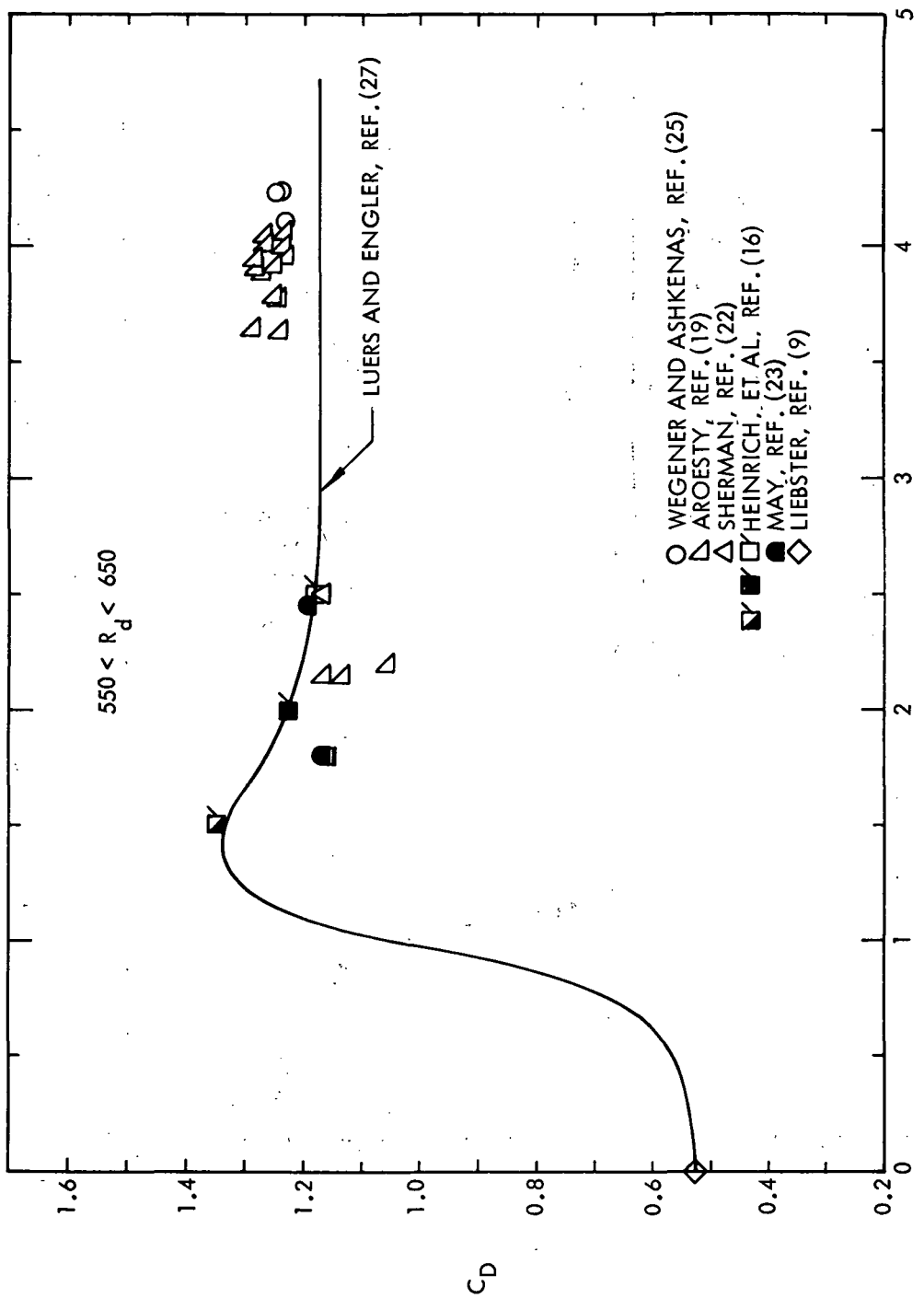

FIG. 14 DRAG COEFFICIENT OF SPHERES NEAR REYNOLDS NUMBER 6×10^2

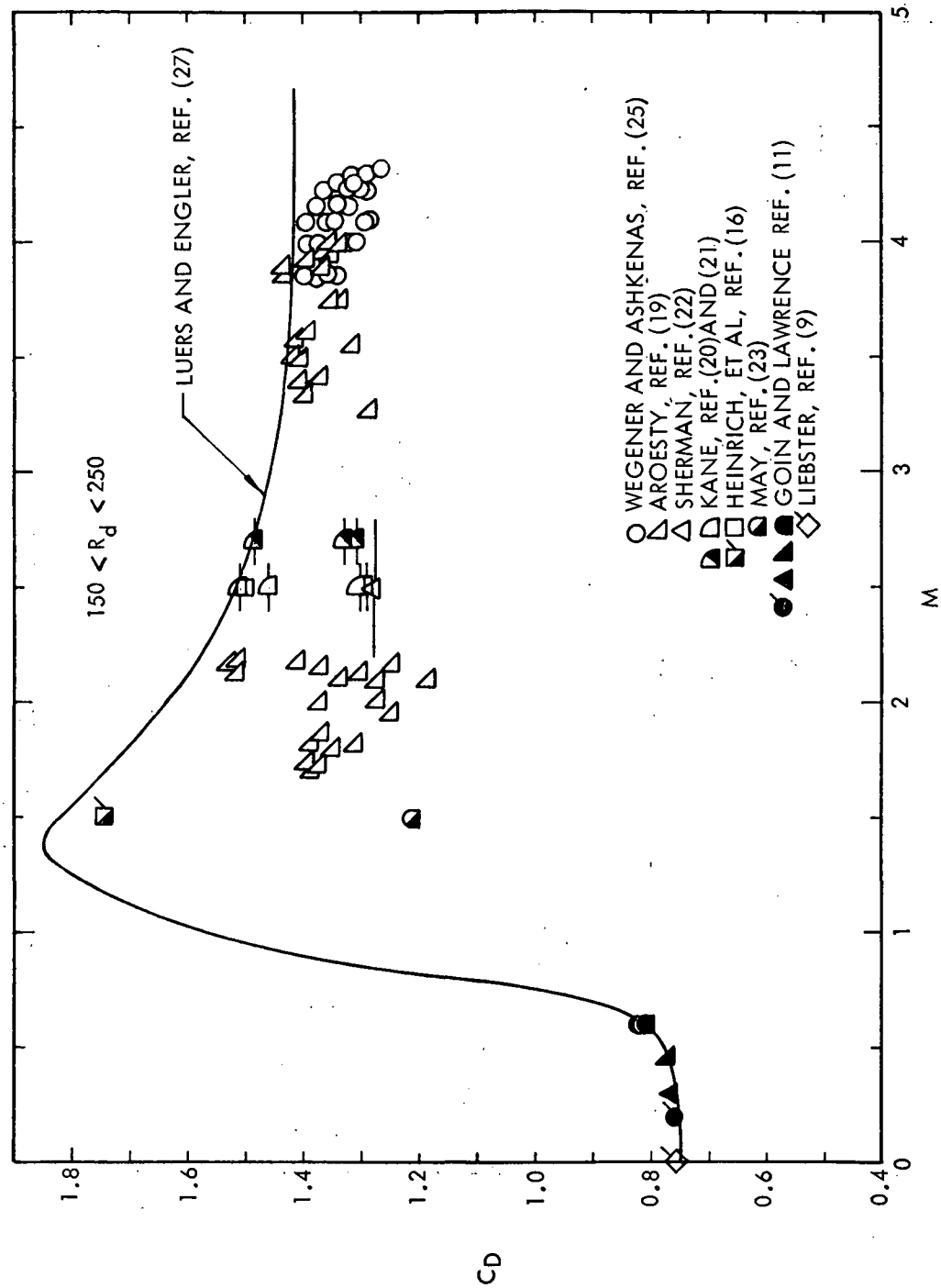

FIG. 15 DRAG COEFFICIENT OF SPHERES NEAR REYNOLDS NUMBER 2×10^2

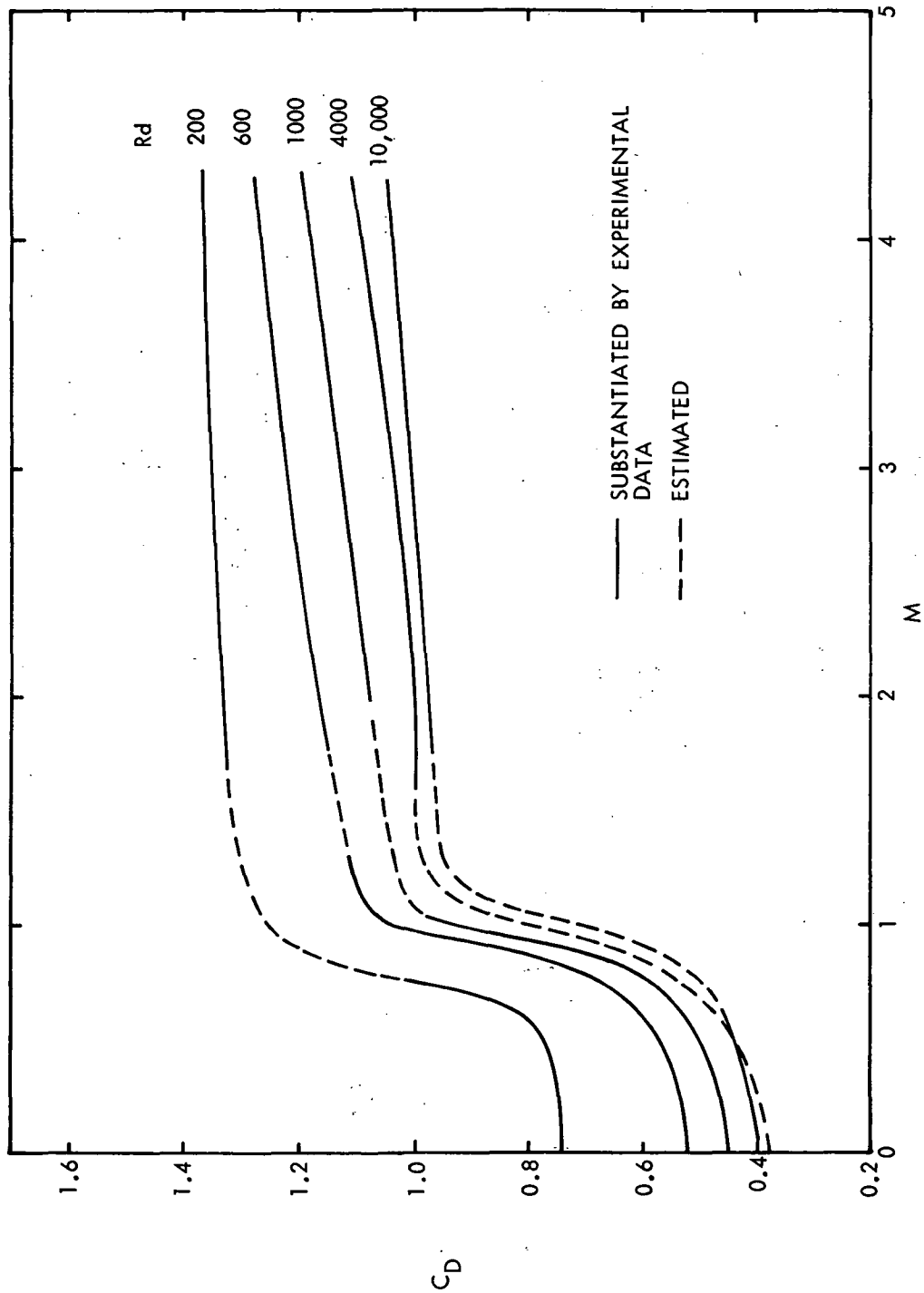

FIG. 16 SUMMARY OF DRAG COEFFICIENT OF SPHERES BASED ON PRESENTLY AVAILABLE DATA

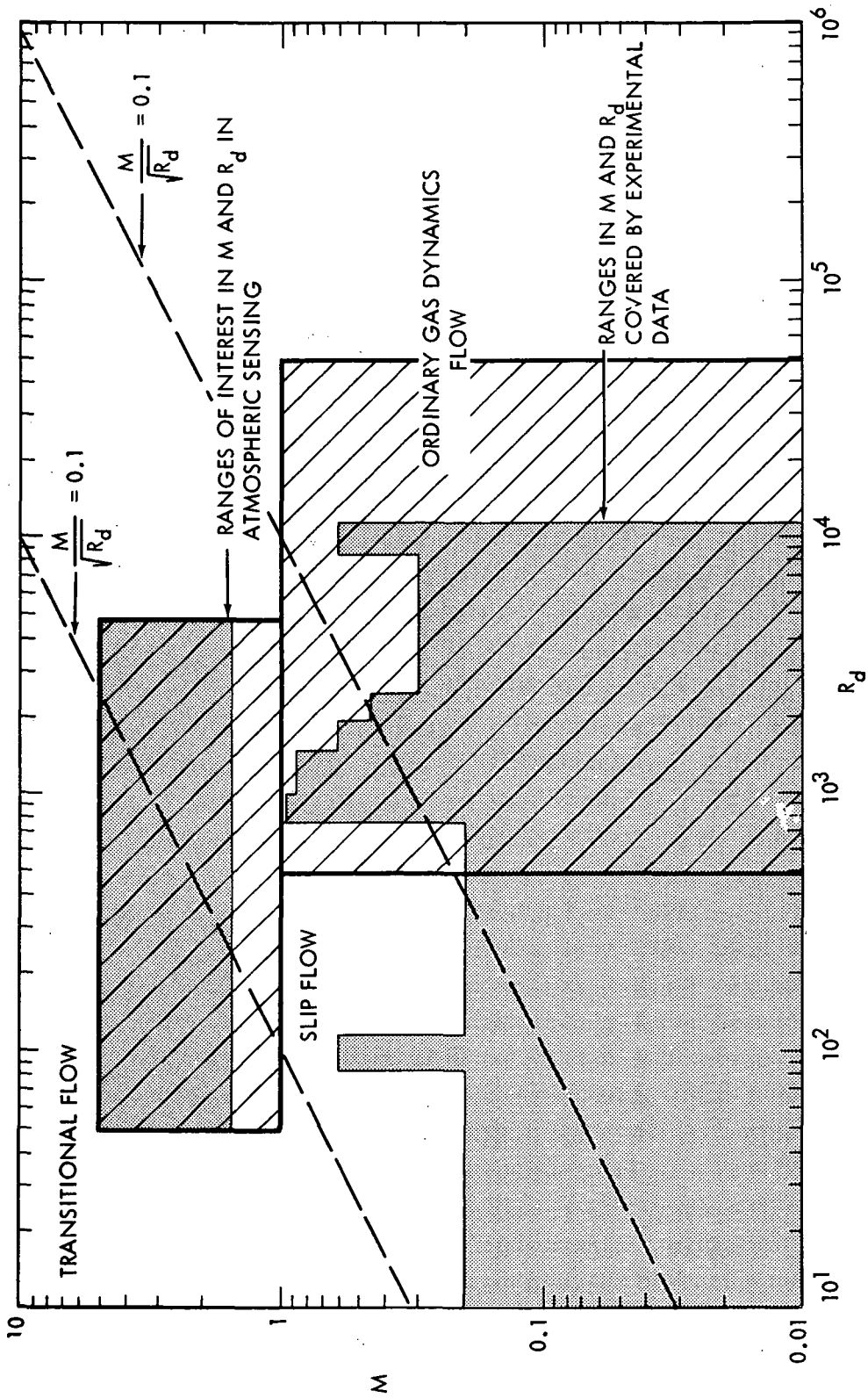

FIG. 17 RANGES OF MACH NUMBER AND REYNOLDS NUMBER FOR WHICH SPHERE DRAG DATA ARE AVAILABLE COMPARED TO THE RANGES OF INTEREST IN THE FALLING SPHERE TECHNIQUE OF ATMOSPHERIC SENSING

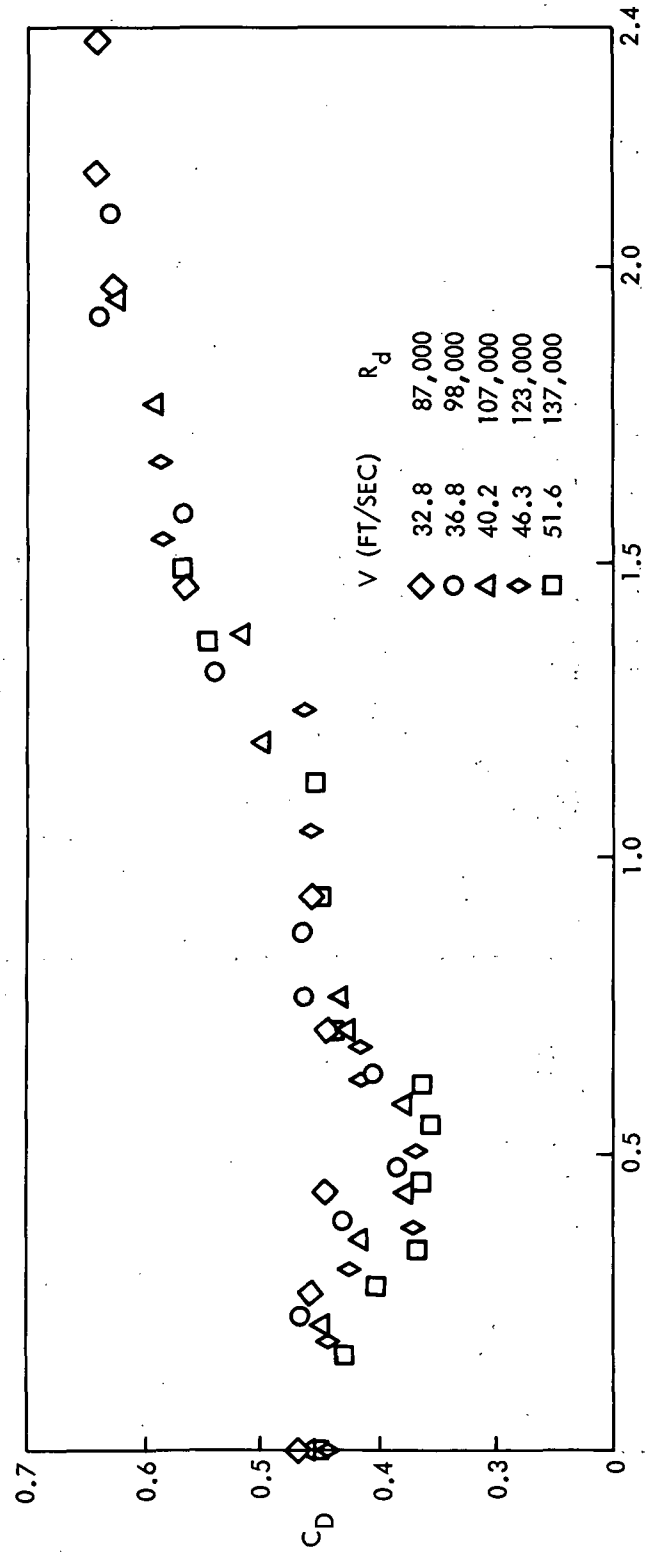

FIG. 18 EFFECT OF ROTATION ON SPHERE DRAG, (HEINRICH, ET AL, REF. (16))

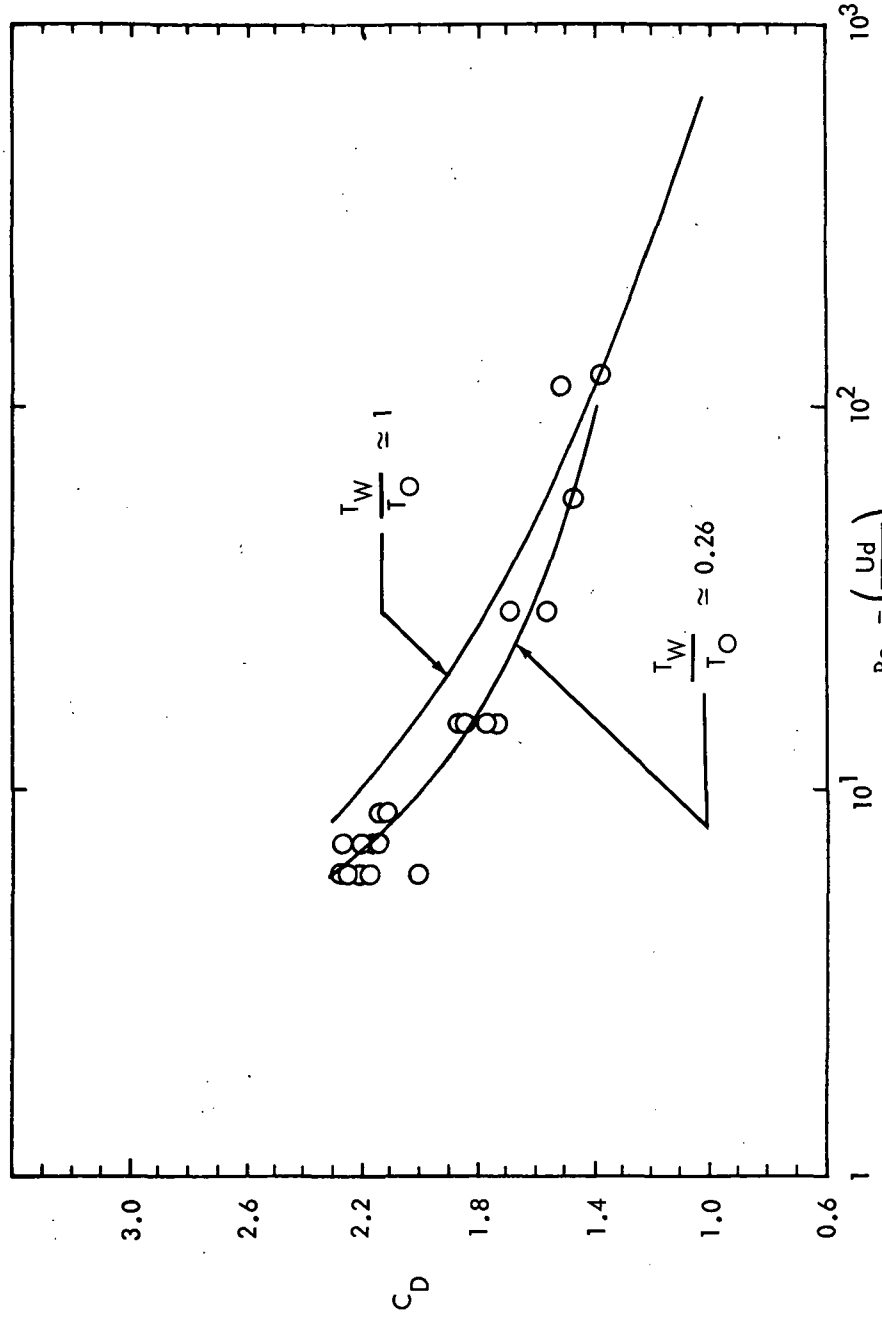

FIG. 19 EFFECT OF WALL TEMPERATURE ON DRAG OF SPHERES NEAR MACH NUMBER 2, (AROESTY, REF.(19))

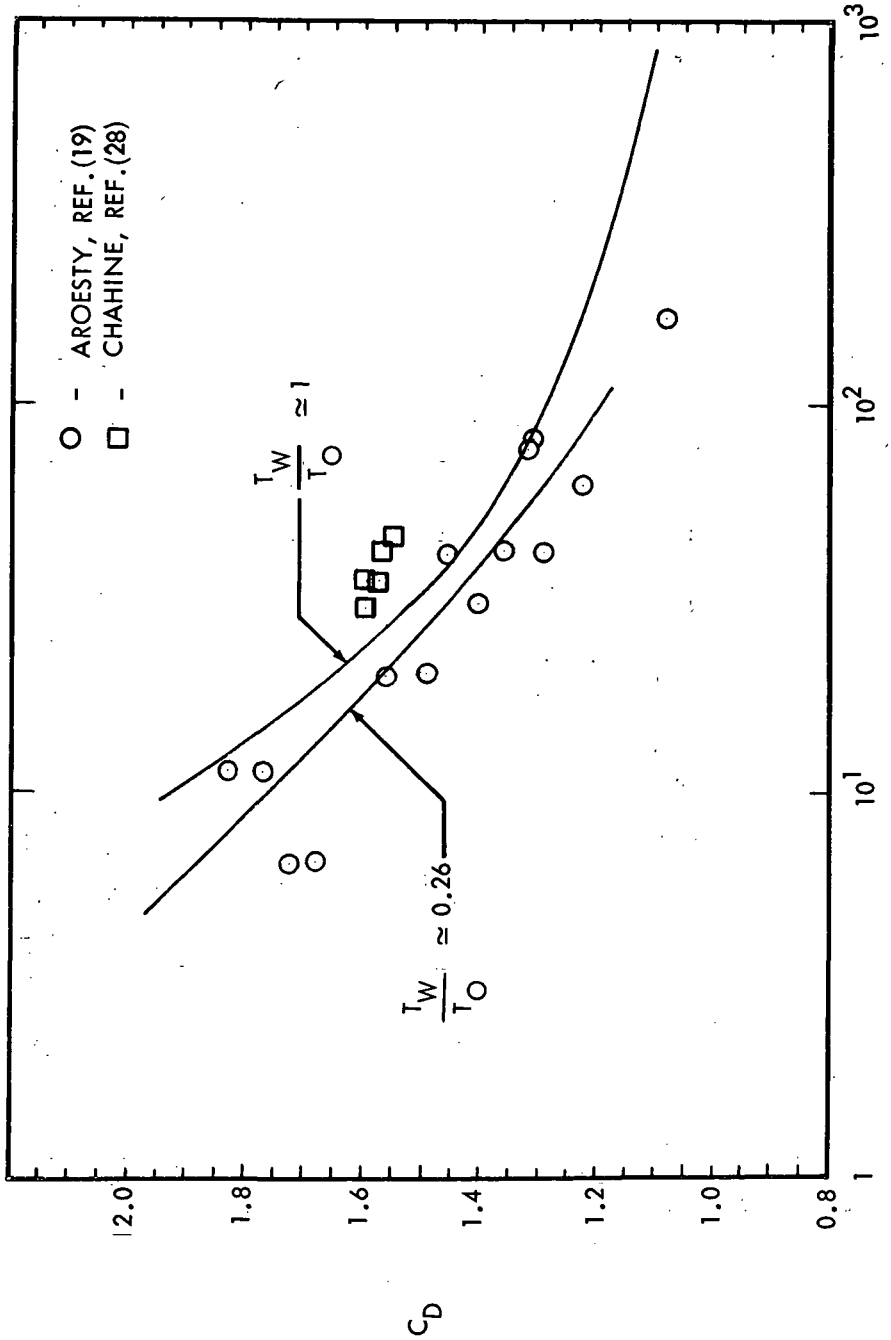

FIG. 20 EFFECT OF WALL TEMPERATURE ON DRAG OF SPHERES NEAR MACH NUMBER 4; (AROESTY, REF. (19))

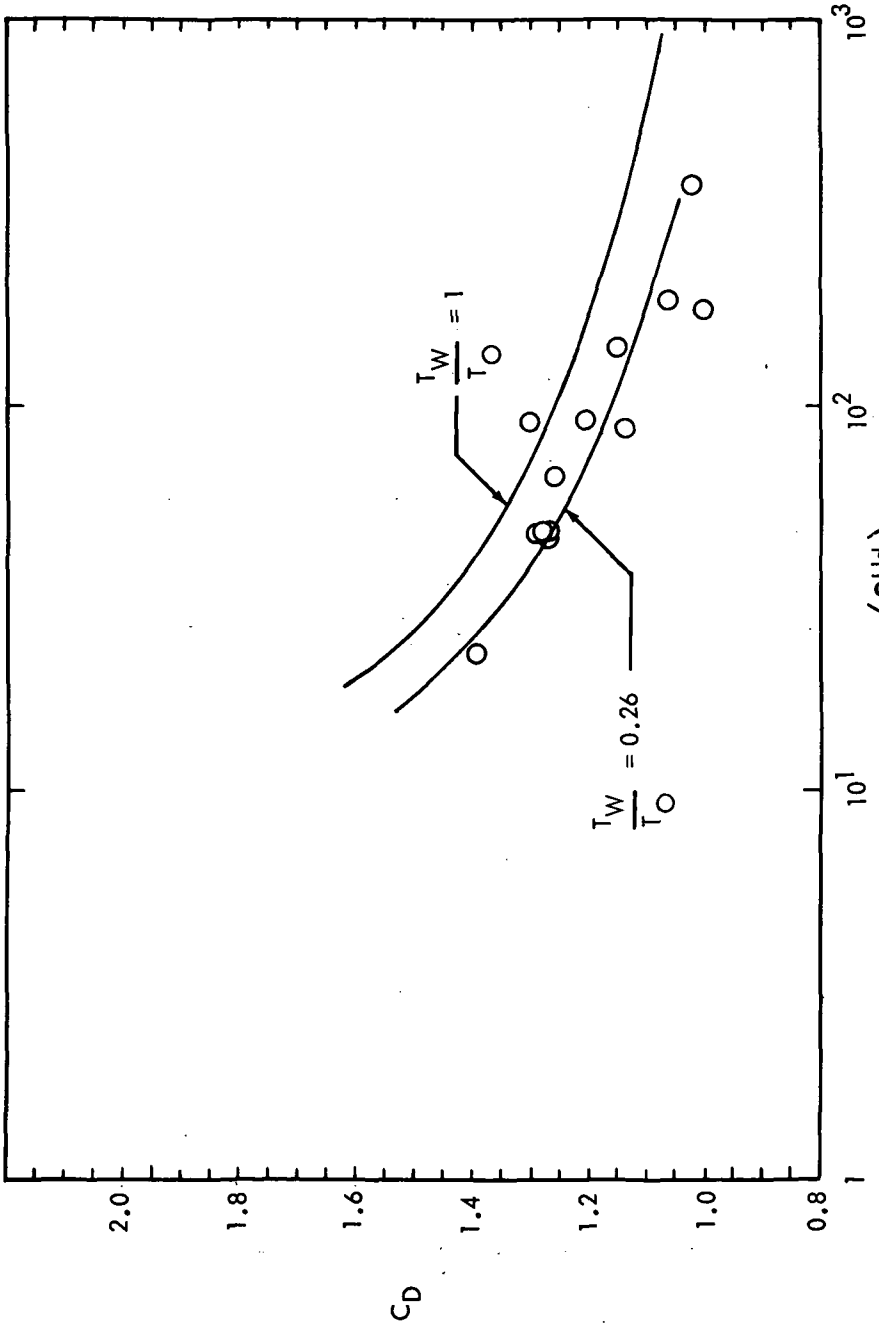

FIG. 21 EFFECT OF WALL TEMPERATURE ON DRAG OF SPHERES NEAR MACH NUMBER 6, (AROESTY, REF. (19))

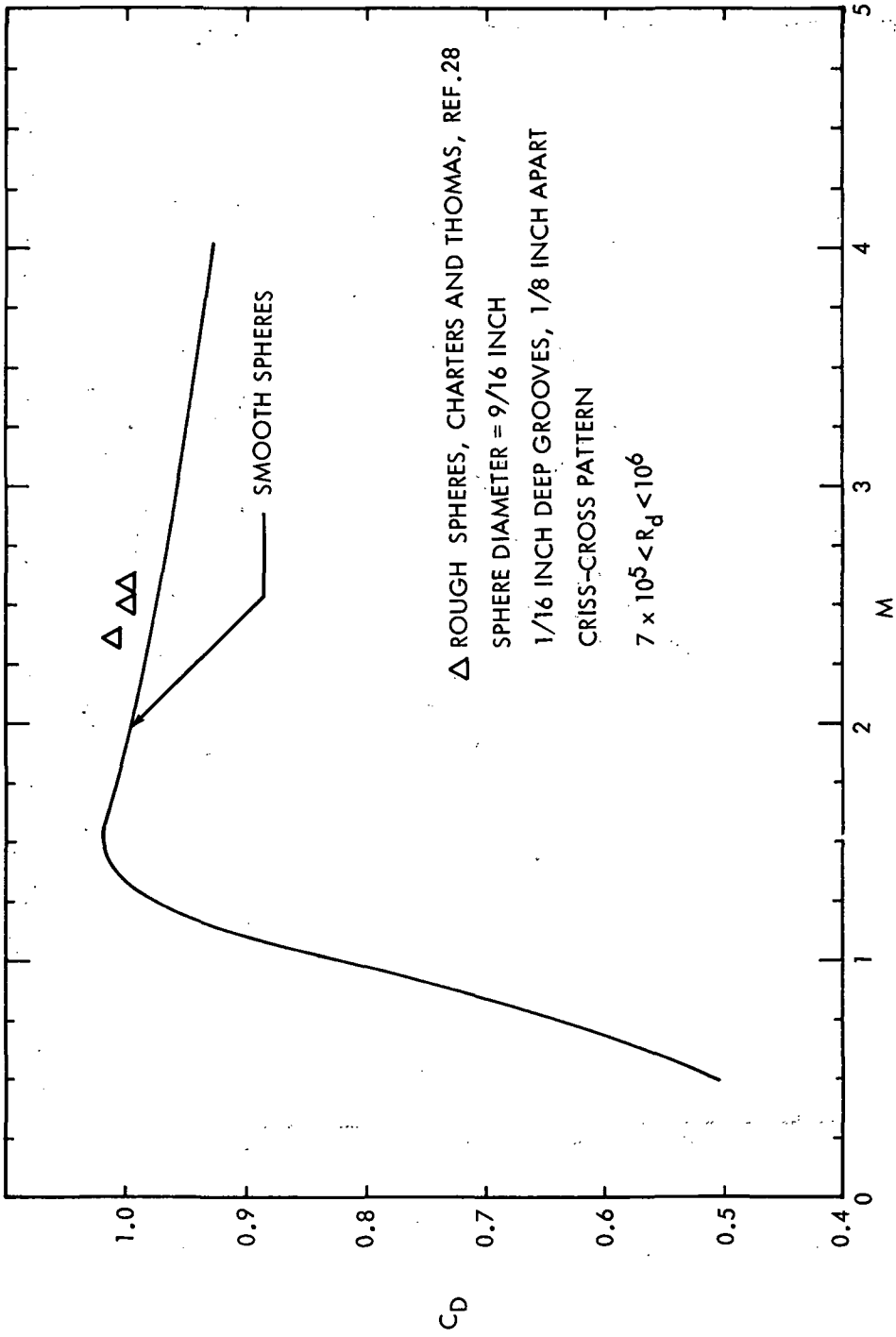

FIG. 22 EFFECT OF ROUGHNESS ON SPHERE DRAG COEFFICIENT AT SUPERSONIC MACH NUMBERS

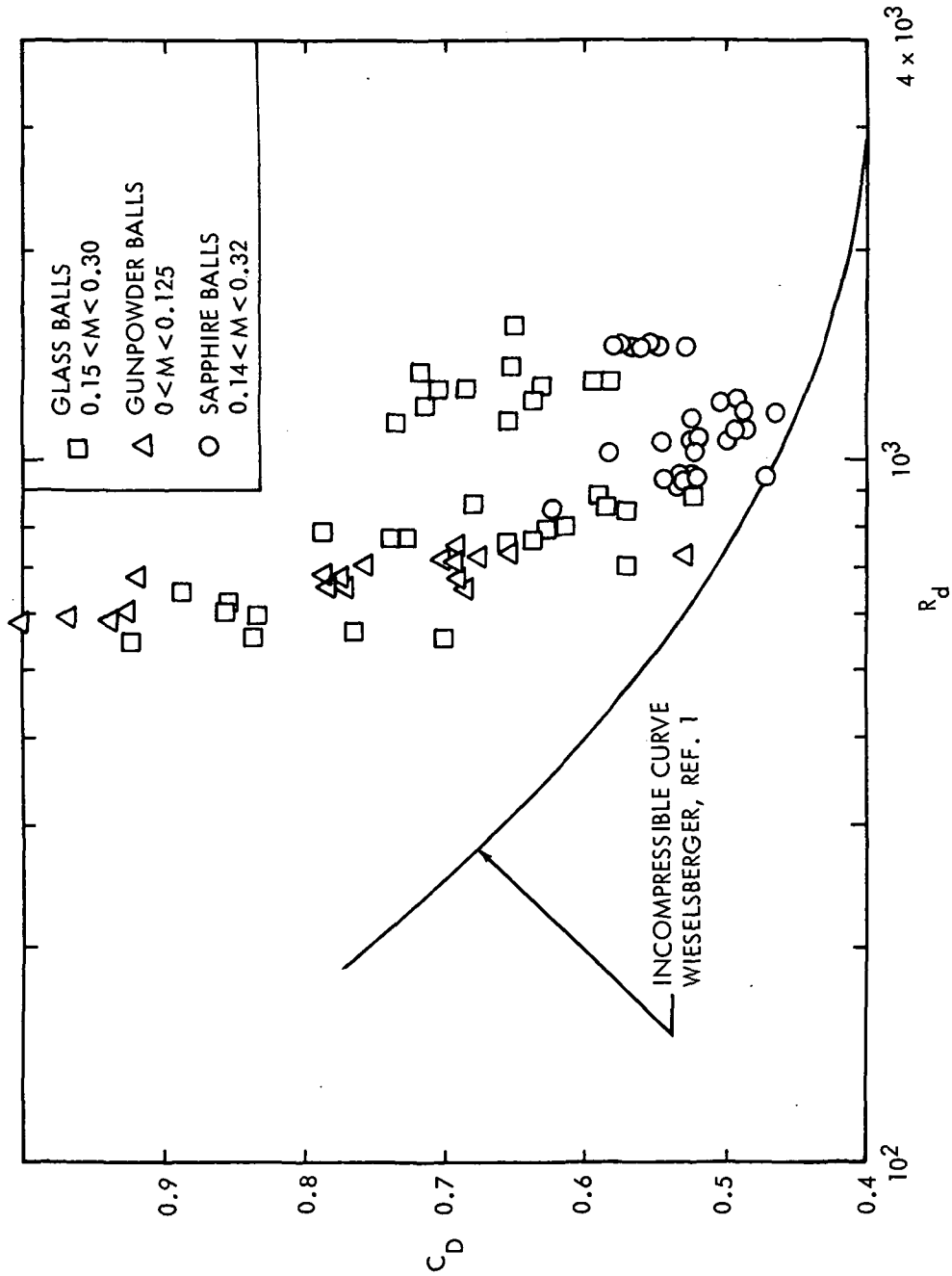

FIG. 23 DRAG COEFFICIENT OF GLASS, GUN POWDER AND SAPHIRE BALLS AT LOW MACH NUMBERS (SELBERG, REF. (31))

DISTRIBUTION

Copies

Commander, Naval Air Systems Command
Department of the Navy
Washington, D. C. 20360
Attn: AIR-604
AIR-5301
AIR-5302
AIR-3032B
AIR-532

Commander, Naval Ordnance Systems Command
Department of the Navy
Washington, D. C. 20360
Attn: ORD-9132
ORD-03A
ORD-035 2
ORD-0321
ORD-05121

Office of Naval Research
Washington, D. C. 20360
Attn: Fluid Dynamics Branch
Structural Mechanics Branch

Ballistic Research Laboratories
Aberdeen Proving Ground, Maryland 21005
Attn: Technical Library, Bldg. 313
Mr. E. D. Boyer, Chief, Transonic Range Facility

Advanced Research Projects Agency
1400 Wilson Boulevard
Arlington, Virginia 22209
Attn: Mr. Clifford E. McLain, Missile Phenomenology Branch

Arnold Engineering Development Center (ARO, Inc.)
Arnold Air Force Station
Tullahoma, Tennessee 37389
Attn: Library/Documents
Mr. A. B. Bailey
Captain Carlos Tierres

Commanding Officer
U. S. Army Mobility Equipment Research and Development Center
Fort Belvoir, Virginia 22060
Attn: Technical Document Center

Commander
Naval Ship Research and Development Center
Bethesda, Maryland 20034
Attn: Library, Aerodynamics Laboratory

Copies

Director
Defense Research and Engineering
The Pentagon
Washington, D. C. 20301
Attn: Library (Technical) 3C-128

Los Alamos Scientific Laboratory
P. O. Box 1663
Los Alamos, New Mexico 87544
Attn: Report Library

National Aeronautics and Space Administration
Lewis Research Center
21000 Brookpark Road
Cleveland, Ohio 44135
Attn: Mr. George Mandel, Chief, Library

National Aeronautics and Space Administration
Goddard Space Flight Center
Greenbelt, Maryland 20771
Attn: Library
Mr. E. F. Sargent, Code 671.2
Mr. J. S. Theon, Code 651

National Aeronautics and Space Administration
George C. Marshall Space Flight Center
Huntsville, Alabama 35812
Attn: R-P&VE-PT, Mr. H. A. Connell
Aero- Astrodynamics Laboratory
Dr. Ernst Geissler

National Aeronautics and Space Administration
Langley Research Center
Langley Station
Hampton, Virginia 23365
Attn: Librarian, MS 185
Mr. Mitchel H. Bertram, MS 243
Mr. Russell Hopko, PARD, MS 213

National Aeronautics and Space Administration
Ames Research Center
Moffett Field, California 94035
Attn: Mr. A. G. Boissevain

Department of Mechanical Engineering
Newark College of Engineering
High Street
Newark, New Jersey 07102
Attn: Dr. W. L. Haberman

Copies

National Bureau of Standards
Washington, D. C. 20234
Attn: Dr. Galen B. Schubauer

Commander
Naval Air Development Center
Warminster, Pennsylvania 18974
Attn: NADC Library

Commander
Naval Missile Center
Point Mugu, California 93041
Attn: Technical Library, Code N0322
Mr. R. Hixon, Code 3250

Commander
Naval Weapons Center
China Lake, California 93555
Attn: Code 406
Code 50704
Technical Library

Superintendent
Naval Postgraduate School
Monterey, California 93940
Attn: Library, Code 0384

Director
Naval Research Laboratory
Washington, D. C. 20390
Attn: Code 2027
Mr. H. F. Swift, Impact Damage Section
Library, Code 2029 (ONRL) 5

Commanding Officer
Naval Underwater Systems Center
Newport, Rhode Island 02844
Attn: Library
Mr. R. J. Grady

Naval Weapons Laboratory
Dahlgren, Virginia 22448
Attn: Library
Code KE
Code TX

NASA Scientific and Technical Information Facility
P. O. Box 33
College Park, Maryland 20740
Attn: NASA Representative (SAK/DL) 2

Copies

Aerospace Corporation
P. O. Box 95085
Los Angeles, California 90045
Attn: Dr. J. S. Whittier

Director
Alden Research Laboratory
Worcester Polytechnic Institute
Worcester, Massachusetts 01609
Attn: Professor L. J. Hooper

Allegany Ballistics Laboratory
Hercules Powder Company
Cumberland, Maryland 21502
Attn: Captain N. J. Kleiss

Applied Physics Laboratory
The Johns Hopkins University
8621 Georgia Avenue
Silver Spring, Maryland 20910
Attn: Dr. Freeman Hill
Mr. L. B. Weckesser
Mr. M. H. Friedman
Document Librarian 6
Dr. L. L. Cronvich

Avco-Everett Research Laboratory
2385 Revere Beach Parkway
Everett, Massachusetts 02149
Attn: Dr. Kantrowitz

Battelle Memorial Institute
505 King Avenue
Columbus, Ohio 43201
Attn: Remote Area Conflict Information Center
Mr. Daniel E. Stohecker

Boeing Company Aerospace Library
P. O. Box 2999
Seattle, Washington 98124
Attn: 8K-38, Mrs. Ruth E. Peerenboom

California Institute of Technology
Pasadena, California 91109
Attn: Professor T. Y. Wu

Copies

The Catholic University of America
Washington, D. C. 20017
Attn: Dr. C. C. Chang, Department of Space
Science and Applied Physics

Ohio State University
Department of Aero- & Astronautical Engineering
2036 Neil Avenue
Columbus, Ohio
Attn: Professor Ting Yi Li

State University of New York at Buffalo
Department of Mechanical Engineering
Buffalo, New York 14214
Attn: Dr. Gordon Hall, Professor of Engineering
and Applied Science

University of Maryland
College Park, Maryland 20742
Attn: Professor A. Wiley Sherwood
Professor John W. Jackson
Professor C. A. Shreeve, Jr.
Dr. Clifford L. Sayre
Dr. Colin H. Marks
Dr. James W. Dally
Professor Robert M. Rivello
Dr. Redfield Allen

General Dynamics/Convair
P. O. Box 1950
San Diego, California 92112
Attn: Mr. R. H. Oversmith, Chief, ASW/Marine Sciences 6-107

General Electric Company
Missile and Space Division
P. O. Box 8555
Philadelphia, Pennsylvania 19101
Attn: Mr. Lawrence I. Chasen, Manager/MSD Libraries 2

Harry Diamond Laboratories
Washington, D. C. 20438
Attn: Library

Marine Bioscience Laboratory
527 Las Alturas Road
Santa Barbara, California 93103
Attn: Dr. A. C. Charters

Copies

Jet Propulsion Laboratory
4800 Oak Grove Drive
Pasadena, California 91103
Attn: Mr. Harry Ashkenas
Library, TDS - Mr. N. E. Devereux

Kaman Aircraft Corporation
Nuclear Division
Colorado Springs, Colorado 80901
Attn: Dr. A. P. Bridges

Lockheed Missiles and Space Company
Missile Systems Division
P. O. Box 504
Sunnyvale, California 94086
Attn: Mr. R. A. Fuhrman, Dept. 81-01, Bldg. 181

North American Aviation, Inc.
Space and Information Systems Division
12214 Lakewood Boulevard
Downey, California 90241
Attn: Technical Information Center, D/096-722 (AJ01)

Sandia Laboratories
Albuquerque, New Mexico 87115
Attn: Mr. R. C. Maydew, Aero-Thermodynamics Dept.
Mr. L. B. Smith

Texas A & M University
Department of Aerospace Engineering
College Station, Texas 77843
Attn: Dr. James L. Rand

University of Cincinnati
Department of Aerospace Engineering
Cincinnati, Ohio 45221
Attn: Dr. Arnold Polak

Sandia Corporation
Livermore Laboratory
P. O. Box 969
Livermore, California 94551
Attn: Technical Library Reference

Director Southwest Research Institute
Department of Mechanical Sciences
San Antonio, Texas 78206
Attn: Library

Copies

National Aeronautics and Space Administration
600 Independence Avenue, S. W.
Washington, D. C. 20546
Attn: Dr. H. H. Kurzweg, Director of Research

Director
St. Anthony Falls Hydraulic Laboratory
University of Minnesota
Minneapolis, Minnesota 55455
Attn: Professor E. Silberman

Stanford University
Department of Aeronautics and Astronautics
Stanford, California 95373
Attn: Dr. Daniel Bershader

Therm Advanced Research, Inc.
100 Hudson Circle
Ithaca, New York 14851

United Aircraft Corporation
Research Laboratories
East Hartford, Connecticut 06108
Attn: Mr. H. J. Charette
Mr. F. S. Owen

Defense Documentation Center
Cameron Station
Alexandria, Virginia 21314 12

University of Delaware
Mechanical and Aeronautical Engineering Department
Newark, Delaware 19711
Attn: Dr. James Danberg

University of Illinois
Department of Theoretical and Applied Mechanics
Talbot Laboratory
Urbana, Illinois 61803
Attn: Mr. R. A. Brocci

University of Utah
College of Engineering
Salt Lake City, Utah 84112
Attn: Professor Max L. Williams, Dean
Dr. R. L. Staffanson
Mr. R. G. Phibbs

Copies

Aerophysics Company
3500 Connecticut Avenue, N. W.
Washington, D. C. 20003
Attn: Mr. Gabriel D. Boehler

University of Wyoming
College of Engineering
University Station, Box 3295
Laramie, Wyoming 82070
Attn: Engineering Library
Professor James D. Matheny, Head,
Department of Mechanical Engineering

National Aeronautics and Space Administration
Langley Research Center
Hampton, Virginia 23365
Attn: Mr. Preisser, Mail Stop 244 10

AMSEL-BL-UA
White Sands Missile Range
White Sands, New Mexico 88001
Attn: Mr. Bob Olsen
Mr. Elton P. Avara

University of Dayton
Dayton, Ohio
Attn: Mr. Nick Engler

Raytheon Company
Wayland, Massachusetts 01778
Attn: Mr. Aaron S. Soltes

National Meteorological Center
Iverson Mall Office Building
Hillcrest Heights, Maryland 20031
Attn: Mr. R. S. Quiroz

University of Michigan
Research Activities Building
Ann Arbor, Michigan 48105
Attn: Mr. F. F. Fischbach

LCV, AF Cambridge Research Laboratories
L. G. Hanscom Field
Bedford, Massachusetts 01730
Attn: Mr. John B. Wright 5

Space Data Corporation
1331 South 26th Street
Phoenix, Arizona
Attn: Mr. Bruce Bollermann

UNCLASSIFIED

Security Classification

DOCUMENT CONTROL DATA - R & D

(Security classification of title, body of abstract and indexing annotation must be entered when the overall report is classified)

1. ORIGINATING ACTIVITY *(Corporate author)* Naval Ordnance Laboratory Silver Spring, Maryland 20910	2a. REPORT SECURITY CLASSIFICATION UNCLASSIFIED 2b. GROUP

3. REPORT TITLE

A REVIEW OF SPHERE DRAG COEFFICIENTS APPLICABLE TO ATMOSPHERIC DENSITY SENSING

4. DESCRIPTIVE NOTES *(Type of report and inclusive dates)*

5. AUTHOR(S) *(First name, middle initial, last name)*

Maigonis V. Krumins

6. REPORT DATE	7a. TOTAL NO. OF PAGES	7b. NO. OF REFS
18 January 1972	59	15

8a. CONTRACT OR GRANT NO.	9a. ORIGINATOR'S REPORT NUMBER(S) NOLTR 72-34
b. PROJECT NO.	
c.	9b. OTHER REPORT NO(S) *(Any other numbers that may be assigned this report)*
d.	

10. DISTRIBUTION STATEMENT

Approved for public release; distribution unlimited.

11. SUPPLEMENTARY NOTES	12. SPONSORING MILITARY ACTIVITY
	National Aeronautics & Space Administration Langley Station, Va. Langley Research Center

13. ABSTRACT

A comprehensive search has been performed on the drag coefficient of spheres in the Reynolds number range from 5×10^1 to 5×10^4 and for Mach numbers up to 5. This Reynolds-Mach number range corresponds to the range of interest in the falling sphere technique of atmospheric sensing. In this technique, the knowledge of the sphere's trajectory and its aerodynamic characteristics are utilized to obtain the density of the atmosphere. The presently available data have been collected and analyzed as to their validity and applicability to atmospheric density measurements. A new drag table is recommended for use in these measurements. Since the vehicles used for atmospheric sensing are inflated spherical balloons, the question still remains if a factor needs to be applied to correct the drag data measured on idealized spheres for effects, such as those due to surface roughness, surface temperature, out of roundness, etc.

DD FORM 1 NOV 65 1473 (PAGE 1)

S/N 0101-807-6801

UNCLASSIFIED

Security Classification

14. KEY WORDS	LINK A		LINK B		LINK C	
	ROLE	WT	ROLE	WT	ROLE	WT
sphere drag atmospheric density sensing						